batteries

MDPI

Review

Molybdenum-Based Electrode Materials Applied in High-Performance Supercapacitors

Yu Wang [1], Hai Wang [2,*] and Gan Qu [1,*]

[1] College of Materials Science and Engineering, Zhengzhou University, Zhengzhou 450001, China; wangyu_0402@163.com
[2] School of Mathematics and Physics, China University of Geosciences, Wuhan 430079, China
* Correspondence: wanghai@cug.edu.cn (H.W.); gqu@zzu.edu.cn (G.Q.)

Abstract: As a novel type of green energy storage device, supercapacitors exhibit several orders of magnitude higher capacities than the traditional dielectric capacitors and significantly higher power density than the traditional secondary batteries. Supercapacitors have been widely applied in energy storage fields. Electrode materials, as pivotal components of supercapacitors, play an important role in electrochemical performance. Molybdenum-based materials have attracted widespread attention for their high theoretical capacitance, abundant resources, and facile synthesis tactics. Therefore, it is necessary to systematically summarize the application of Mo-based electrode materials in high-performance supercapacitors and unveil their developmental direction and trends. In this paper, we provide a review of binary Mo-based materials, ternary Mo-based materials, nanocomposites of Mo-based materials, and Mo-based MOFs and derivative materials. In addition, we further point out the key issues on the development of Mo-based materials in supercapacitors. This review may inspire more insightful works and enlighten other electrochemical areas concerning Mo-based materials.

Keywords: supercapacitors; Mo-based electrode materials; high performance; binary materials; ternary material; nanocomposites; MOFs

check for updates

Citation: Wang, Y.; Wang, H.; Qu, G. Molybdenum-Based Electrode Materials Applied in High-Performance Supercapacitors. *Batteries* **2023**, *9*, 479. https://doi.org/10.3390/batteries9090479

Academic Editor: Pascal Venet

Received: 19 August 2023
Revised: 16 September 2023
Accepted: 19 September 2023
Published: 21 September 2023

1. Introduction

The energy crisis and environmental pollution are the two principal themes in the world. Therefore, renewable clean energy sources, such as wind, solar, and tidal energy, have attracted much attention in the energy fields [1]. However, the development of clean energy is limited by space and time factors [2]. Consequently, effective energy storage systems are needed to promote their commercial application. Among electrochemical energy storage devices, supercapacitors stand out for their high-power density and long cycle life [3,4].

The history of capacitors can be traced back to 1746, while the invention of the Leiden bottle is a pivotal milestone. A typical capacitor comprises two closely aligned conductors separated by an insulating medium. The stored energy of the capacitor is positively related to the voltage until the threshold of breakdown voltage [5]. In 1975, Conway et al. [6] claimed that the charge and discharge behaviors of RuO_2 closely resemble capacitors rather than batteries, and termed them "supercapacitors".

Supercapacitors can be classified into two main types: electric double layer supercapacitors (EDLCs) and pseudocapacitors. EDLCs stored charge through ion adsorption and desorption on the surface of electrodes. Therefore, EDLCs often show long lifespan and high energy efficiency, because there are only physical reactions on the surface during the charge and discharge processes [7]. In contrast, pseudocapacitive supercapacitors undergo reversible redox reactions in the interior part of the electrode materials [8]. Therefore, pseudocapacitive electrodes often present higher specific capacitance and energy density than those of EDLCs.

Generally, a supercapacitor comprises four components: current collector, electrode, electrolyte, and separator [9]. The electrode material plays a pivotal role in determining the specific capacitance and energy density. As a result, the design and regulation of electrode materials have become the focus in the field of supercapacitors [10–14].

China is rich in molybdenum resources. The element of Mo exhibits variable valence states (+4, +5, and +6) [15]. In addition, Mo-based materials exhibit pronounced electrochemical activity, which have been widely investigated in recent years [16–18]. As shown in Figure 1, Mo-based electrode materials can be categorized as binary Mo-based materials (MoO_2, MoO_3), ternary Mo-based materials ($NiMoO_4$, $CoMoO_4$, and $MnMoO_4$, etc.), nanocomposites of Mo-based materials (Mo_2C@CNT and MoS_2/graphene), and Mo-based MOFs and Mo-based materials deriving from MOF materials (Mo-MOF/PANI and BiMo-MOF).

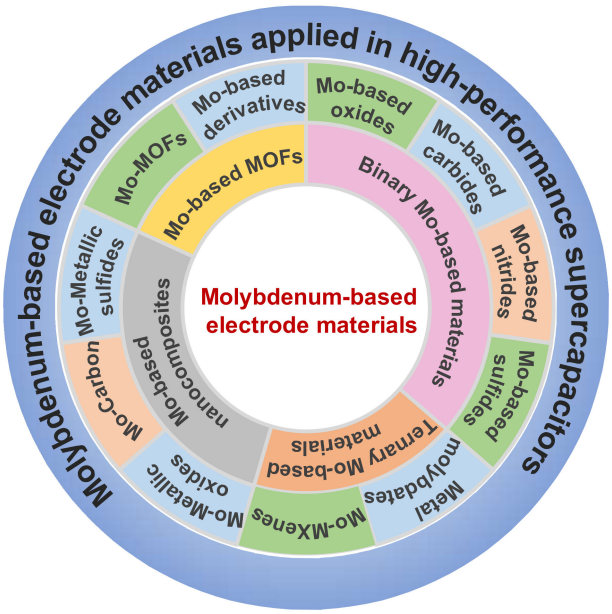

Figure 1. A series of Mo-based electrode materials for supercapacitors.

In this review, we provide a detailed summary of the research progress on binary, ternary, nanocomposite, and Mo-based MOFs and derivative materials. We also address the urgent issues on the design and exploit of Mo-based electrode materials in future. This discussion offers valuable insights into the study of Mo-based electrode materials applied in supercapacitors.

2. Mo-Based Electrode Materials for Supercapacitors

2.1. Binary Mo-Based Materials

Binary Mo-based materials are composed of two different types of elements, for example MoO_3, Mo_2C, MoN, and MoS_2, etc., which have attracted extensive research into supercapacitors.

2.1.1. Molybdenum Oxides

Molybdenum oxides mainly include MoO_2, MoO_3, and MoO_{3-x}, which are composed of MoO_6 octahedra through edge or corner sharing [19].

MoO_3 usually exists in three crystal types: α-MoO_3, β-MoO_3, and h-MoO_3. α-MoO_3 belongs to the orthorhombic crystal system, in which MoO_6 octahedra are connected with each other through weak van der Waals forces along the [010] direction and corner sharing along the [100] direction [20]. β-MoO_3 belongs to the monoclinic crystal system, in which MoO_6 octahedra are connected through corner sharing [21]. h-MoO_3 belongs to the hexagonal crystal system, in which MoO_6 octahedra share edges along the [001] direction

and corners along the [100] direction [22]. Therefore, h-MoO_3 shows a zig-zag structure with a cavity of ~3 Å in diameter allowing for the insertion/deinsertion of ions [23]. Prakash et al. [24] employed the solution combustion method to synthesize a series of α-MoO_3 nanorods at different combustion temperatures. The SEM image in Figure 2a illustrates the morphology of α-MoO_3, which shows one-dimensional nanorods with a diameter of 50 nm and length of several micrometers. The α-MoO_3 nanorods show a specific capacitance of 176 F g^{-1} at 1 mA g^{-1}. Even after 1000 cycles, the capacitance retention reaches 92%. Additionally, Niu et al. [25] synthesized the h-MoO_3 nanorods and nanoparticles using a hydrothermal method, as shown in Figure 2b. The nanorod structure facilitates adequate contact between the electrode materials and electrolyte, thereby improving the electrochemical performance. As a result, the MoO_3 nanorods achieved a specific capacitance of 229.0 F g^{-1} at 0.2 A g^{-1}. Zhu et al. [26] fabricated MoO_3 nanoplates by the heat-treating of C_3N_4 and ammonium molybdate (Figure 2c). The extended layered structure enables the rapid insertion/deinsertion of ions. Notably, a high specific capacitance of 994.2 F g^{-1} was achieved at 0.5 A g^{-1}. Moreover, the assembled YP50//MoO_3 device shows a capacitance retention of 84% after 1500 cycles at 3 A g^{-1}.

MoO_2 belongs to the monoclinic crystal system, in which the twisted MoO_6 octahedra units are connected to each other along the [001] direction by sharing edges. The distorted structure induces a change in the electronic state of Mo, leading to metallic conductivity [27]. Ma et al. [28] synthesized MoO_2 nanoparticles using a hydrothermal method (Figure 2d) and explored their electrochemical behavior in acid electrolytes. The charge storage behavior of MoO_2 under acidic conditions is ascribed to the surface redox reactions (Faradaic capacitance) and ion intercalation/deintercalation reactions (battery capacitance). However, the electrochemical mechanism of MoO_2 is ascribed to the electric double layer capacitors' behavior under the neutral electrolyte. Notably, the MoO_2 electrode exhibited a specific capacitance of 509.8 F g^{-1} at 0.5 A g^{-1} in a 0.5 M H_2SO_4 solution. Additionally, the morphological structure of MoO_2 is also investigated to improve its capacitive performance. Wu et al. [29] synthesized hierarchical mesoporous MoO_2 spheres using a hydrothermal method (Figure 2e). The MoO_2 nanospheres exhibit a specific surface area of 29.5 m^2 g^{-1}, facilitating ion contact and improvement in charge transfer resistance. As a result, the specific capacitance reaches 381.0 F g^{-1} at 0.3 A g^{-1}. Furthermore, the crystal structure of MoO_2 is further researched to reveal its influence on the performance of supercapacitors. Zhao et al. [30] introduced amorphous domains into MoO_2 nanosheets (Figure 2f), which enhances the ion diffusion and electron transport. Under a current density of 5 A g^{-1}, the capacitance retention remains 85% after 4000 cycles.

Non-stoichiometric MoO_{3-x}($0 < x < 1$) enhances the intrinsic conductivity and increases the concentration of free carriers due to the introduced oxygen vacancies [31]. In comparison with MoO_3 (3.2 eV), the bandgap of MoO_{3-x} is reduced to 2.9 eV, which is expected to favor improved capacitance performance [32]. There have been many strategies to construct MoO_{3-x}. In addition, the size and shape adjustment of oxygen-deficient molybdenum oxides is relatively mature. At present, the reported methods mainly include the template method [33], surfactant method [34], solvothermal method [35], and sol–gel method [36], etc. Wu et al. [35] successfully synthesized MoO_{3-x} nanobelts with oxygen vacancy concentration of up to 20%. Figure 2g illustrates the MoO_{3-x} nanobelts, which show 30–40 nm in thickness and 100–200 nm in width. This structural design reduces the migration distance of electrolyte ions and enhances the availability of internal active sites. Notably, the MoO_{3-x} nanobelt exhibits a remarkable specific capacitance of 1,220 F g^{-1} at 50 A g^{-1} and shows an impressive capacitance retention of nearly 100% even after 38,000 cycles. Bai et al. [37] synthesized α-MoO_{3-x} nanobelts via a facile one-pot hydrothermal approach (Figure 2h). The enlarged interlayer spacing could weaken the interlamellar Van der Waals force, facilitating the rapid diffusion of ions. The α-MoO_{3-x} nanobelts exhibit a specific capacitance of 912.5 F g^{-1} at 1 A g^{-1}. Salkar et al. [38] synthesized two-dimensional MoO_{3-x} microplates and microdisks. The SEM images illustrate the morphological structures in Figure 2i. According to the experimental data, the improved

capacitor performance stems from the introduction of oxygen vacancies, the high specific surface area, and the enlarged layered structures. The MoO_{3-x} microplates and microdisks display specific capacitances of 410 F g^{-1} and 226 F g^{-1} at 20 A g^{-1}, respectively. Impressively, the capacitance retention is above 90% and the coulombic efficiency is above 98% after 10,000 cycles. The electrochemical performances of some reported molybdenum oxides are presented in Table 1.

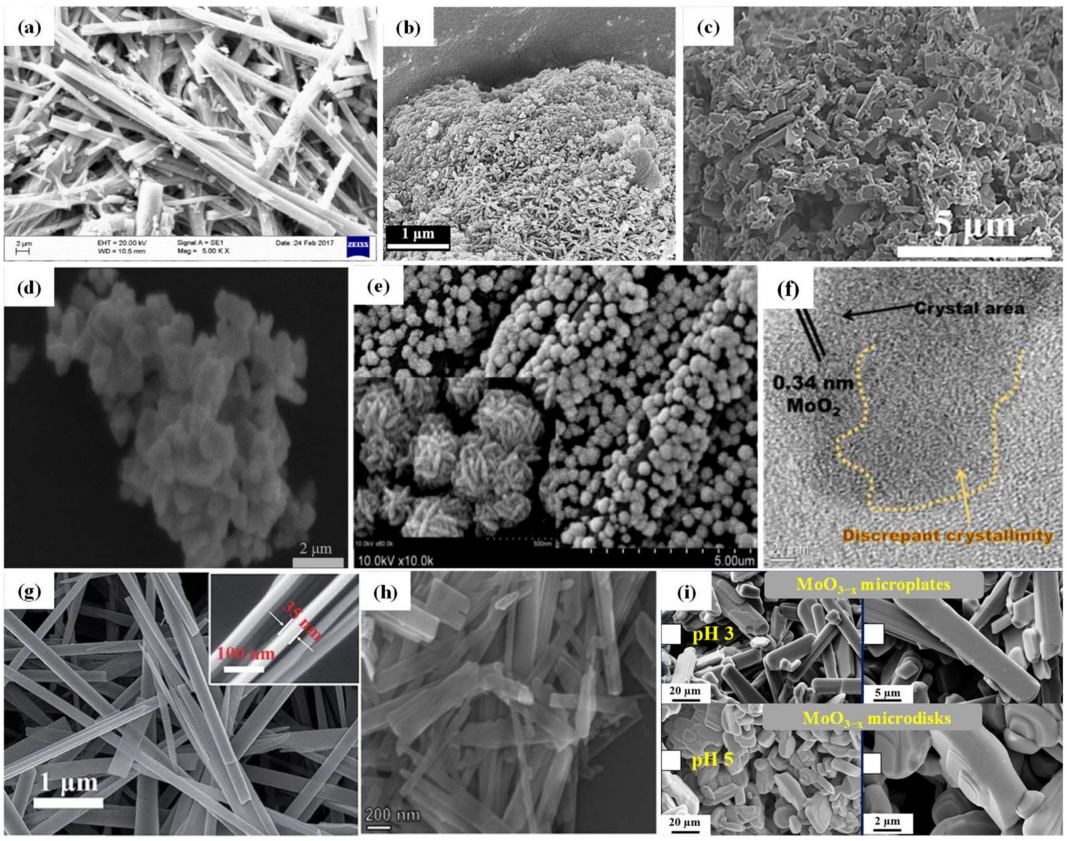

Figure 2. SEM images. (**a**) MoO_3 nanorods. Reprinted with permission from [24]. Copyright 2018, Elsevier. (**b**) h-MoO_3 nanorods and nanoparticles. Reprinted with permission from [25]. Copyright 2020, Elsevier. (**c**) MoO_3 nanoplates. Reprinted with permission from [26]. Copyright 2023, Elsevier. (**d**) MoO_2 nanoparticles. Reprinted with permission from [28]. Copyright 2022, Elsevier. (**e**) Mesoporous MoO_2 spheres. Reprinted with permission from [29]. Copyright 2019, Elsevier. (**f**) MoO_2 nanosheets. Reprinted with permission from [30]. Copyright 2018, Royal Society of Chemistry. (**g**) MoO_{3-x} nanobelts. Reprinted with permission from [35]. Copyright 2019, Royal Society of Chemistry. (**h**) MoO_{3-x} nanobelts. Reprinted with permission from [37]. Copyright 2022, Elsevier. (**i**) MoO_{3-x} microplates and microdisks. Reprinted with permission from [38]. Copyright 2018, Elsevier.

2.1.2. Molybdenum Carbides

Transition metal carbides (TMCs) possess high electrical conductivity, and have been widely studied in energy storage, catalysis, and electromagnetic shielding fields. Now, the reported TMCs mainly include NbC [39], VC [40], TiC [41], and Mo_2C [42], etc. Notably, Mo_2C has been widely investigated in supercapacitors.

Yu et al. [43] conducted simulation calculations to analyze the electronic properties of molybdenum carbide. The energy band structure and projected DOS are presented in Figure 3a. For the molybdenum carbides (MoC, Mo_2C, MoC_2), an increase in the proportion of C means a reduction in free electrons on the surface. Mo_2C with the smallest proportion of C and numerous dangling bonds on the surface shows significant potential as an electrode material in supercapacitors. Illustrated in Figure 3b, Xu et al. [42]

successfully synthesized lamellar Mo_2C through the calcination of amine–metal oxides, yielding ultrafine nanoparticles of ~10 nm. This microstructural design is beneficial for the adequate contact between the electrode and electrolyte, facilitating improved performance. Remarkably, a specific capacitance of 88 F g^{-1} has been achieved at 0.5 A g^{-1}. In addition, the asymmetric Mo_2C//AC capacitor displays an impressive capacitance retention of 95% after 1200 cycles and an energy density of 44.1 W h kg^{-1}. The electrochemical performances of some reported molybdenum carbides are presented in Table 2.

Table 1. The electrochemical performances of molybdenum oxide materials.

Electrode Material	Method	Structure	Specific Capacitance	Capacitance Retention	Ref.
α-MoO_3	solution combustion	nanorods	176 F g^{-1} (1 mA g^{-1})	92%, 1000 cycles	[24]
h-MoO_3	hydrothermal	nanorods and nanoparticles	229.0 F g^{-1} (0.2 A g^{-1})	N/A	[25]
MoO_3	heat-treating	nanoplates	994.2 F g^{-1} (0.5 A g^{-1})	84%, 1500 cycles	[26]
MoO_2	hydrothermal	nanoparticles	509.8 F g^{-1} (0.5 A g^{-1})	64.5%, 2500 cycles	[28]
MoO_2	hydrothermal	mesoporous	381.0 F g^{-1} (0.3 A g^{-1})	82.4%, 1000 cycles	[29]
MoO_2	hydrothermal	nanosheets	243 mA h g^{-1} (0.1 A g^{-1})	85%, 4000 cycles	[30]
MoO_{3-x}	hydrothermal	nanobelts	1,220 F g^{-1} (50 A g^{-1})	100%, 38,000 cycles	[35]
α-MoO_{3-x}	hydrothermal	nanobelts	912.5 F g^{-1} (1 A g^{-1})	N/A	[37]
MoO_{3-x}	liquid phase	microplates and microdisks	410 F g^{-1} (20 A g^{-1})	90%, 12,000 cycles	[38]

(N/A = unavailable).

2.1.3. Molybdenum Nitrides

Transition metal nitrides (TMNs) have received extensive attention in the energy storage and catalysis fields due to their high electrical conductivity and robust chemical stability [44]. Xiao et al. [45] employed the salt template method to synthesize MoN nanosheets, as demonstrated in Figure 3c. The MoN nanosheets exhibit a negligible band gap and an exceptional electronic conductivity, thereby improving the electrochemical performance. Notably, the volume-specific capacitance reaches 928 F cm^{-3} at 2 mV s^{-1}, while maintains 200 F cm^{-3} even under 20 mV s^{-1}. Gao et al. [46] prepared zig-zag γ-Mo_2N thin film by magnetron sputtering. The SEM image is presented in Figure 3d. The zig-zag structured γ-Mo_2N presents an outstanding area capacitance of 248 mF cm^{-2} at 50 mV s^{-1}. After 20,000 cycles at 200 mV s^{-1}, a remarkable capacitance retention of 95% is achieved. In addition, the symmetrical solid-state γ-Mo_2N//γ-Mo_2N device delivers an excellent power density of 107.1 W cm^{-3} at 33.8 mW h cm^{-3}. Djire et al. [47] synthesized face-centered cubic γ-Mo_2N with high surface area through high-temperature treatment of molybdenum source and ammonia gas, as illustrated in Figure 3e. The pseudocapacitive charge storage mechanism was conducted through in situ experiments. As a result, the simultaneous insertion of hydrogen ions (H^+) and electrons (e^-) into the material leads to the reduction in Mo during the electrochemical processes. The γ-Mo_2N shows a high specific capacitance of 1500 F g^{-1} with a potential window of 1.2 V in aqueous acidic electrolytes. The electrochemical performances of some reported molybdenum nitrides are presented in Table 2.

2.1.4. Molybdenum Sulfides

Molybdenum chalcogenides possess a layered structure, in which the large interlayer spaces are convenient for the storage and transport of ions [48]. This layered characteristic renders them an ideal candidate as an energy storage material. Molybdenum sulfide (MoS_2) and molybdenum selenide ($MoSe_2$) stand out in molybdenum chalcogenides. The high intrinsic ionic conductivity facilitates improved electrochemical performance. MoS_2 displays layered S-Mo-S stacks under van der Waals interactions [49]. There are two distinct phase states: the metallic 1T phase and the semiconducting 2H phase. The 1T phase easily

transforms into the 2H phase due to its thermodynamic instability. MoS_2 predominantly exists in the form of the 2H phase in nature [50]. The active sites of the 2H phase are mainly distributed along the sulfur edge, while those of the metallic 1T phase are mainly distributed along both the edge and basal plane, inherently favoring the electrochemical process [51].

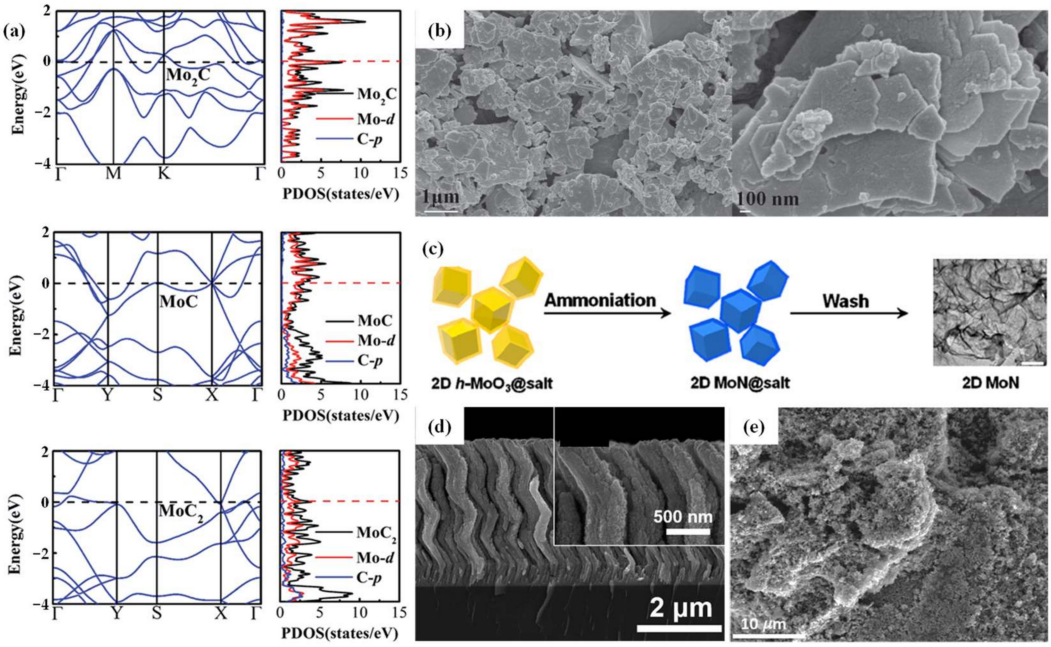

Figure 3. (**a**) Calculated band structures and projected DOS for Mo_2C, MoC, and MoC_2. Reprinted with permission from [43]. Copyright 2019, Royal Society of Chemistry. (**b**) SEM image of Mo_2C nanosheets. Reprinted with permission from [42]. Copyright 2018, IOP Publishing. (**c**) Schematic diagram of the synthesis of MoN nanosheets. Reprinted with permission from [45]. Copyright 2017, American Chemical Society. (**d**) SEM image of zig-zag γ-Mo_2N films. Reprinted with permission from [46]. Open access. (**e**) SEM image of γ-Mo_2N. Reprinted with permission from [47]. Copyright 2018, Elsevier.

Liu et al. [52] used a simple one-step hydrothermal method to obtain rosette-like MoS_2 nanoflowers (Figure 4a). Figure 4b presents the GCD curves of MoS_2 nanoflowers at varying current densities; they exhibit a specific capacitance of 137 mF cm^{-2} at 10 mA cm^{-2}. After 10,000 cycles, the capacitance retention reaches 81.6%. Teli et al. [53] reported amorphous MoS_2 nanoflakes (Figure 4c) using one-step electrodeposition, achieving a specific capacitance of 416.9 mF cm^{-2} at 1 mA cm^{-2}. An asymmetric device was assembled using activated carbon and MoS_2 as negative and positive electrodes, respectively; this exhibited an area capacitance of 277.3 mF cm^{-2} and energy density of 0.15 mW h cm^{-2} at 5.33 mW cm^{-2}. Furthermore, 90.1% cyclability and excellent coulombic efficiency measured up to 3000 cycles were observed for an asymmetric device (Figure 4d). Additionally, Joseph et al. [54] prepared defect-rich 1T-MoS_2 nanosheets, which exhibited a specific capacitance of 379 F g^{-1} at a current density of 1 A g^{-1}. The assembled supercapacitor device delivered an energy density of 21.3 W h kg^{-1} and a power density of 750 W kg^{-1}. The capacitance retention remains 92% even after 3000 cycles (Figure 4e). Gupta et al. [55] utilized a hydrothermal method to synthesize MoS_2 nanoflowers. The surface features of the flakes and wrinkles facilitate the intercalation and deintercalation of cations. Notably, a specific capacitance of 255.65 F g^{-1} is achieved at a current density of 0.25 A g^{-1}. Impressively, even after 1000 cycles, 70% of the initial specific capacitance is retained (Figure 4f).

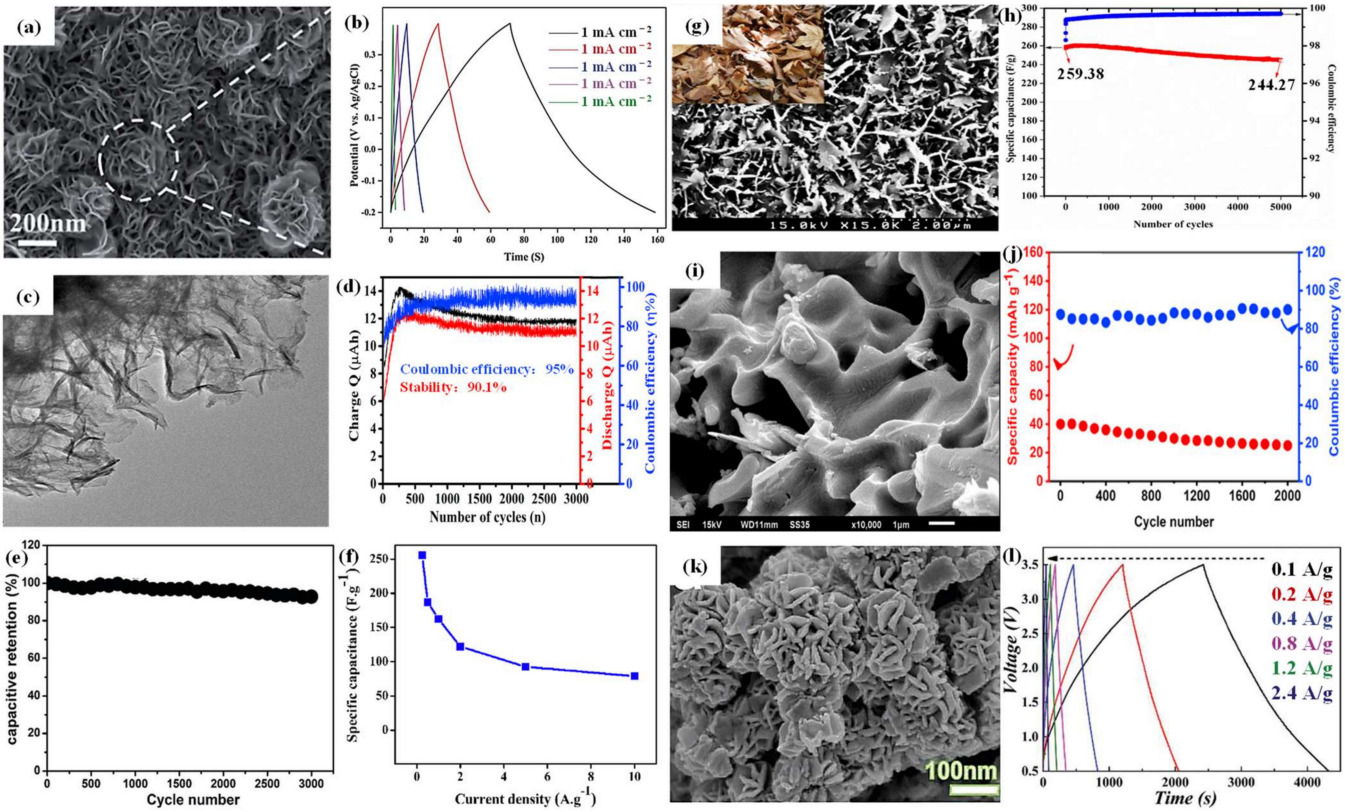

Figure 4. (**a**) SEM image of MoS_2 nanoflowers; (**b**) GCD curves of MoS_2 nanoflowers at different current densities. Reprinted with permission from [52]. Copyright 2019, Royal Society of Chemistry. (**c**) TEM image of MoS_2 nanoflakes; (**d**) cyclic performance of MoS_2 nanoflakes at 3 mA cm^{-2}. Reprinted with permission from [53]. Copyright 2022, Elsevier. (**e**) Cyclic performance of 1T-MoS_2 nanosheets at 5 A g^{-1}. Reprinted with permission from [54]. Copyright 2018, Royal Society of Chemistry. (**f**) Specific capacitance of MoS_2 nanoflowers at different current densities. Reprinted with permission from [55]. Copyright 2020, Elsevier. (**g**) SEM image of mesoporous $MoSe_2$; (**h**) cyclic performance of mesoporous $MoSe_2$ at 1 A g^{-1}. Reprinted with permission from [56]. Copyright 2019, Elsevier. (**i**) SEM image of 2H-$MoSe_2$; (**j**) cyclic performance of 2H-$MoSe_2$ at 5 A g^{-1}. Reprinted with permission from [57]. Copyright 2020, Elsevier. (**k**) SEM image of $MoSe_2$ nanoflowers; (**l**) CV curves of $MoSe_2$ nanoflowers at different current densities. Reprinted with permission from [58]. Copyright 2019, Royal Society of Chemistry.

The atomic structure of $MoSe_2$ closely resembles that of MoS_2, comprising three atomic layers held together by weak van der Waals interactions. Consequently, $MoSe_2$ has attracted considerable interest as a potential electrode material in supercapacitors [59].

$MoSe_2$ with a mesoporous structure shows a large specific surface area, providing significant benefits for ion transport. Vattikuti et al. [56] successfully synthesized a uniform dry leaf-like mesoporous $MoSe_2$ nanostructure using a microwave-assisted method, as illustrated in Figure 4g. The as-prepared leaf-like perforated $MoSe_2$ exhibited remarkable capacitance of 257.38 F g^{-1} at 1 A g^{-1} with a capacitance retention of almost 95% after 5000 cycles, see Figure 4h. In comparison to the mesoporous configuration, $MoSe_2$ with a nanosheet structure further increases the specific surface area, shortens the ion diffusion path, and improves the electrochemical performance. Upadhyay et al. [57] reported the synthesis of layered 2H-$MoSe_2$ nanosheets via an in situ selenization route. The SEM image is shown in Figure 4i. The $MoSe_2$ nanosheet exhibits a specific capacitance of 46.22 mA h g^{-1} at 2 A g^{-1}. Remarkably, even after 2000 cycles at a current density of 5 A g^{-1}, a capacitance retention of 64% was observed (Figure 4j). Additionally, the nanoflower structure would offer ample channels for electrolyte diffusion during the electrochemical processes. Zhang et al. [58] synthesized smooth and irregular pleated flower-like $MoSe_2$ using a facile hydrothermal method. The SEM image is

displayed in Figure 4k. Furthermore, Figure 4l illustrates the CV curves of $MoSe_2$ at different current densities. Notably, the specific capacitance reaches 641.5 mA h g^{-1} at a current density of 0.1 A g^{-1}. The assembled hybrid $MoSe_2$//AC capacitors displayed a high energy density of 78.75 W h kg^{-1} and a high power density of 3600 W kg^{-1}. In addition, the capacity retention rate is 70.28% after 5000 cycles with a potential window of 0.5–3.5 V. The electrochemical performances of some reported molybdenum sulfides are presented in Table 2.

Table 2. The electrochemical performances of molybdenum carbide, molybdenum nitride, and molybdenum sulfide materials.

Electrode Material	Method	Structure	Specific Capacitance	Capacitance Retention	Ref.
Mo_2C	calcination	nanosheets	88 F g^{-1} (0.5 A g^{-1})	95%, 1200 cycles	[42]
MoN	template	nanosheets	928 F cm^{-3} (2 mV s^{-1})	95%, 25,000 cycles	[45]
γ-Mo_2N	magnetron sputtering	thin films	248 mF cm^{-2} (50 mV s^{-1})	95%, 20,000 cycles	[46]
γ-Mo_2N	calcination	porous	1500 F g^{-1} (N/A)	N/A	[47]
MoS_2	hydrothermal	nanoflowers	137 mF cm^{-2} (10 mA cm^{-2})	81.6%, 10,000 cycles	[52]
MoS_2	electrodeposition	nanosheets	416.9 mF cm^{-2} (1 mA cm^{-2})	90.1%, 3000 cycles	[53]
2H-MoS_2	hydrothermal	nanosheets	379 F g^{-1} (1 A g^{-1})	92%, 3000 cycles	[54]
MoS_2	hydrothermal	nanoflowers	255.65 F g^{-1} (0.25 A g^{-1})	70%, 1000 cycles	[55]
$MoSe_2$	microwave	mesoporous	257.38 F g^{-1} (1 A g^{-1})	95%, 5000 cycles	[56]
2H-$MoSe_2$	in situ selenization	nanosheets	46.22 mA h g^{-1} (2 A g^{-1})	64%, 2000 cycles	[57]
$MoSe_2$	hydrothermal	nanoflowers	641.5 mA h g^{-1} (0.1 A g^{-1})	70.28%, 5000 cycles	[58]

(N/A = unavailable).

2.2. Ternary Mo-Based Materials

Ternary Mo-based materials are composed of three elements, including metal molybdates and MXenes. The synthesis pathway of metal molybdate is simple and low cost while exhibiting remarkable physical and chemical properties [60]. MXenes exhibit a characteristic two-dimensional layered structure, offering a high specific surface area and exceptional electrical conductivity [61]. Notably, ternary Mo-based materials have been widely researched for supercapacitors in recent years.

2.2.1. Metal Molybdates

Metal molybdates, for example $MMoO_4$ (M = Cu [62], Zn [63], Bi [64], Ni [65], Mn [66], Sn [67], Co [68], etc.), constitute a significant category in inorganic materials.

Farahpour et al. [62] conducted a single-pot hydrothermal method to grow $CuMoO_4$ nanosheets on nickel foam. In Figure 5a, the prepared $CuMoO_4$ nanosheets are uniformly distributed with grass-like morphology. The specific capacitance of $CuMoO_4$ reached 2259.55 F g^{-1} at 1 A g^{-1}. The cyclic stability analysis showed a capacitance retention of 90.08% at 16 A g^{-1} after 5000 cycles. Moreover, the $CuMoO_4$//AC supercapacitor device displayed a high energy density of 52.51 W h kg^{-1} at 600 W kg^{-1}. In addition, the device exhibited a capacitance retention of 78.6% after 5000 cycles at 4 A g^{-1} (Figure 5b). Gurusamy et al. [63] produced a series of rod-shaped $ZnMoO_4$ using a template method by optimizing the concentration of CTAB. The schematic diagram of the synthesis process is presented in Figure 5c. The rod-like $ZnMoO_4$ material showed an impressive specific capacitance of 779 F g^{-1} at 5 mV s^{-1} and retained 90% of the initial capacitance even after 3000 cycles at 100 mV s^{-1}. Additionally, Yesuraj et al. [64] employed the hydrothermal method with a DNA template to synthesize Bi_2MoO_6 nanoplates, as depicted in Figure 5d. The Bi_2MoO_6 nanoplates with a large number of small nanoparticles (5–7 nm) on their surface result in an increased surface area, which facilitated charge transport and ion diffusion. The Bi_2MoO_6 exhibited a high specific capacitance of 698 F g^{-1} at 5 mV s^{-1}, along with a capacitance retention of 86% even after 3000 cycles at a high scan rate of 100 mV s^{-1} in 1 M NaOH electrolyte. Qu et al. [65] presented a rapid and zero-energy consumption method to obtain metal molybdate nanowires in supercapacitors (Figure 5e). The synthesized $NiMoO_4$ nanowires exhibited an impressive specific capacitance of 549 C g^{-1} at 1 A g^{-1}. Furthermore, the assembled supercapacitor device demonstrated a specific capacitance of 156 F g^{-1} at

0.8 A g^{-1}, along with an energy density of 55.6 W h kg^{-1} at 640 W kg^{-1}. Additionally, Sheng et al. [66] employed a solid-state chemical synthesis approach to produce 1D $MnMoO_4$ $0.9H_2O$ and $MnMoO_4$ nanorods (Figure 5f), which exhibited a specific capacitance of 210.2 F g^{-1} at 1 A g^{-1}. Notably, the $MnMoO_4$ nanorods displayed remarkable cycle stability, maintaining a cycle life of 112.6% even after 10,000 cycles. Furthermore, the electrochemical performance of $MnMoO_4$ underwent substantial enhancement upon the removal of crystal water from $MnMoO_4{\cdot}0.9H_2O$, leading to a noteworthy 2.4-fold increase in specific capacitance. Remarkably, the asymmetric supercapacitor device achieved a high energy density of 23.5 W h kg^{-1} at 187.4 W kg^{-1}. This remarkable electrochemical performance is attributed to the elevated electrical conductivity from the 1D nanostructure after the removal of crystallization water. Sakthikumar et al. [67] optimized the ratio of CTAB to metal salt and reaction conditions to synthesize sheet-like $Sn(MoO_4)_2$, as shown in the SEM image in Figure 5g. The specific capacitance of flake $Sn(MoO_4)_2$ is 109 F g^{-1} at 5 mV s^{-1} and the capacitance retention reaches 70% after 4000 cycles at 8 mV s^{-1}. Li et al. [68] synthesized $CoMoO_4$ material in situ on nickel foam using a hydrothermal method (Figure 5h). The prepared $CoMoO_4$ shows a cuboid rod-like structure with loose folds on the periphery, enhancing the contact between the electrode and electrolyte, and thereby facilitating ion diffusion and transmission. At a current density of 3 mA cm^{-2}, the discharge capacitance of $CoMoO_4$ reaches 11.112 F cm^{-2}. The electrochemical performances of some reported metal molybdates are presented in Table 3.

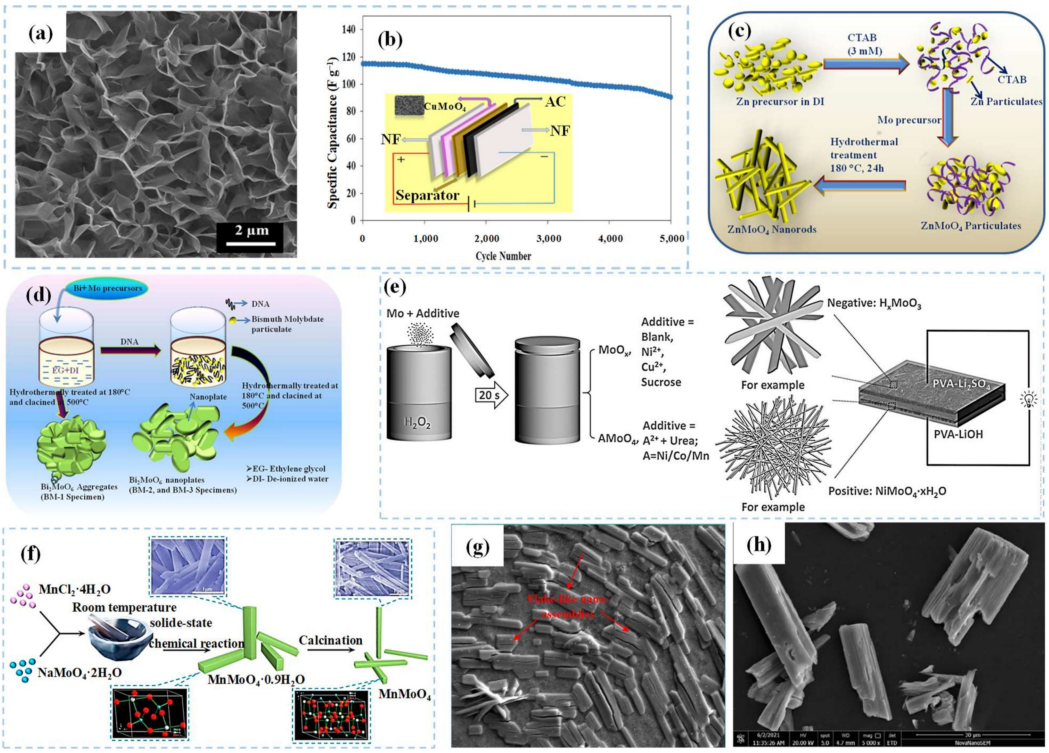

Figure 5. (**a**) SEM image of $CuMoO_4$ nanosheets; (**b**) cyclic performance of $CuMoO_4$//AC at 4 A g^{-1}. Reprinted with permission from [62]. Copyright 2021, Elsevier. (**c**) Schematic diagram of the synthesis of $ZnMoO_4$ nanorods. Reprinted with permission from [63]. Copyright 2020, Springer Nature. (**d**) Schematic diagram of the synthesis of Bi_2MoO_6 nanoplates. Reprinted with permission from [64]. Copyright 2019, Elsevier. (**e**) Schematic diagram of the synthesis of $NiMoO_4{\cdot}xH_2O$ nanowires. Reprinted with permission from [65]. Copyright 2017, John Wiley and sons. (**f**) Schematic diagram of the synthesis of $MnMoO_4$ nanorods. Reprinted with permission from [66]. Copyright 2021, Elsevier. (**g**) SEM image of $Sn(MoO_4)_2$ nanosheets. Reprinted with permission from [67]. Copyright 2016, Royal Society of Chemistry. (**h**) SEM image of $CoMoO_4$ nanorods. Reprinted with permission from [68]. Copyright 2022, Springer Nature.

2.2.2. Mo-MXenes

In recent years, two-dimensional transition metal carbonitride (MXene) materials have attracted extensive attention in the energy storage field, owing to their unique physical and chemical characters [69]. The MAX phase is classified as a layered carbide or nitride and is characterized by the chemical formula $M_{n+1}AX_n$ (n = 1~3). Here, M represents various transition metal elements, including Sc, Ti, Zr, Nb, Ta, Cr, Mo, etc. X stands for carbon and/or nitrogen, while A refers to a main group element. Through etching, A can be removed from the MAX phase, leading to the formation of a graphene-like MXene structure. The structural chemical formula of MXenes is $M_{n+1}X_nT_x$ (n = 1~3), where T represents a functional group such as O, F, or OH [70]. The distinctive properties of MXene materials have sparked interest from researchers in supercapacitors.

Halim et al. [71] firstly put forward a large-scale synthesis strategy for 2D Mo_2CT_x flakes. LiF/HCl acts as an etchant to selectively etch Ga from Mo_2Ga_2C powder, leading to a delamination process, as depicted in Figure 6a. The obtained Mo_2CT_x flakes exhibit high conductivity and effective intersheet conduction due to their dense stacking. At a scan rate of 2 mV s^{-1}, the specific capacitance reaches 700 F cm^{-3}, while the capacitance retention is nearly 100% even after 10,000 cycles at 10 A g^{-1} (Figure 6b). Das et al. [72] conducted a theoretical analysis on the structure of Mo_2CO_2 to predict the electronic structure and investigate its capacitive behavior. As a result, the functionalized MXenes induce a change in charge transfer dynamics. Therefore, H inclines to form covalent bonds with O, leading to the sharing of electrons. Impressively, the theoretically calculated capacitance of Mo_2CO_2 is closely consistent with the experimental results. Zheng et al. [73] prepared $Mo_{1.33}CT_z$ i-MXene films with a vacancy structure by etching $(Mo_{0.66}Sc_{0.33})_2AlC$, as illustrated in Figure 6c. The inclusion of vacancies notably optimizes the ion transport. Notably, the $Mo_{1.33}CT_z$ i-MXene attained an energy density of 25.4 mW h cm^{-3} at a power density of 152.4 mW cm^{-3} in a 15 M LiBr electrolyte, as depicted in Figure 6d. Even after 20,000 cycles at 100 mV s^{-1}, 99.4% of the initial specific capacitance is retained (Figure 6e). The electrochemical performances of some reported Mo-MXenes are presented in Table 3.

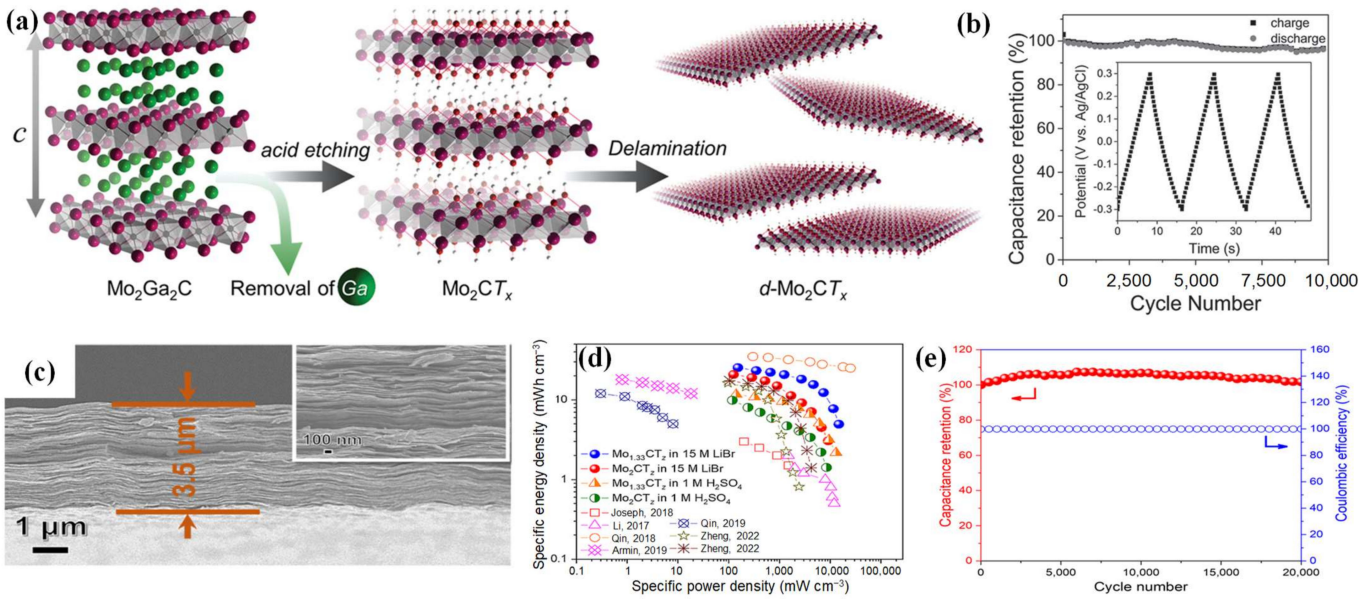

Figure 6. (**a**) Schematic diagram of the synthesis of Mo_2CT_x; (**b**) cyclic performance of Mo_2CT_x at 10 A g^{-1}. Reprinted with permission from [71]. Copyright 2016, John Wiley and sons. (**c**) SEM image of $Mo_{1.33}CT_z$; (**d**) Ragone diagram of $Mo_{1.33}CT_z$ in 1 M H_2SO_4 and 15 M LiBr compared to different Mxene [74–79]; (**e**) cyclic performance of $Mo_{1.33}CT_z$ at 100 mV s^{-1}. Reprinted with permission from [73]. Copyright 2020, Elsevier.

Table 3. The electrochemical performances of metal molybdates and Mo-MXene materials.

Electrode Material	Method	Structure	Specific Capacitance	Capacitance Retention	Ref.
$CuMoO_4$	hydrothermal	nanosheets	2259.55 F g^{-1} (1 A g^{-1})	90.08%, 5000 cycles	[62]
$ZnMoO_4$	template	nanorods	779 F g^{-1} (5 mV s^{-1})	90%, 3000 cycles	[63]
Bi_2MoO_6	template	nanoplates	698 F g^{-1} (5 mV s^{-1})	86%, 3000 cycles	[64]
$NiMoO_4 \cdot xH_2O$	mixture	nanowires	549 C g^{-1} (1 A g^{-1})	81%, 5000 cycles	[65]
$MnMoO_4$	nitriding	nanorods	210.2 F g^{-1} (1 A g^{-1})	112.6%, 10,000 cycles	[66]
$Sn(MoO_4)_2$	solution method	nanosheets	109 F g^{-1} (5 mV s^{-1})	70%, 4000 cycles	[67]
$CoMoO_4$	hydrothermal	nanorods	11.11 F cm^{-2} (3 mA cm^{-2})	N/A	[68]
Mo_2CT_x	etching	nanosheets	700 F cm^{-3} (2 mV s^{-1})	~100%, 10,000 cycles	[71]
$Mo_{1.33}CT_z$	etching	nanofilms	127 F cm^{-3} (2 mV s^{-1})	99.4%, 20,000 cycles	[73]

(N/A = unavailable).

Currently, numerous reports discuss the application of MXene materials in supercapacitors; however, few studies focus on Mo-based MXenes. Based on the articles reviewed above, it is evident that Mo-based MXenes exhibit exceptional performance in supercapacitors. Therefore, this review presents a promising research direction in supercapacitors.

2.3. Nanocomposites of Mo-Based Materials

Nanocomposites of Mo-based materials are obtained by combining Mo-based materials with other nanomaterials. The synergistic effects from different components can enhance the performance of supercapacitors, attracting the attention of researchers.

2.3.1. Nanocomposites of Mo-Based Materials and Metallic Oxides

The research progress concerning a specific type of Mo-based material has been previously discussed. Recently, researchers have undertaken efforts to combine Mo-based materials with a variety of metal oxides, aiming at enhancing the electrochemical performance. Typical metal oxides used in the composites mainly include MnO_2, Cr_2O_3, Fe_3O_4, TiO_2, Co_3O_4, VO_x, and ZnO, etc. [80–84].

MnO_2 serves as an optimal material to combine with Mo-based electrode materials, owing to its high energy density. As depicted in Figure 7a, Hu et al. [80] fabricated a MoS_2/MnO_2 heterostructure. This architecture effectively avoided the re-deposition and aggregation of two-dimensional materials, leading to a significant increase in the electrochemically active surface area and thereby enhancing the electrochemical performance. At a current density of 2 A g^{-1}, its specific capacitance reaches 275 F g^{-1}. The MoS_2/MnO_2 demonstrates improved cyclic stability, retaining 89% of its initial specific capacitance even after 10,000 cycles at 10 A g^{-1}. Furthermore, Cr_2O_3, with a resistivity of 1.5×10^{-8} Ω cm and robust mechanical attributes, was combined with Mo-based materials to produce flexible supercapacitors. Sharma et al. [81] employed magnetron sputtering technology to synthesize Cr_2O_3-MoO_2 nanosheets (Figure 7b), exhibiting a specific capacitance of 340.8 F g^{-1} at a current density of 2 mA cm^{-2}. The assembled Cr_2O_3-MoO_2//C device delivers an operating voltage of 1.9 V and achieves a specific capacitance of 74.5 F g^{-1} at 2 mA cm^{-2}. In addition, the specific energy density reaches 37.35 W h kg^{-1} at a specific power of 9708 W kg^{-1}. The capacitance retention rate is 91.7% after 20,000 cycles. Fe_3O_4 has several advantages, such as high theoretical specific capacitance, cost-effectiveness, and high conductivity (2×10^4 S m^{-1}) compared to most other metal oxides. Li et al. [82] prepared Fe_3O_4-MoO_2 hybrid nanofilms, where MoO_2 is uniformly distributed on the surface of Fe_3O_4. The spinel Fe_3O_4 nanorods grow on the current collector, ensuring rapid electron transport. Moreover, the gap among the nanorods facilitates electrolyte penetration, leading to small interfacial resistance. The Fe_3O_4-MoO_2 exhibits a specific capacitance of 65.0 mF cm^{-2} at 2 mV s^{-1}, showing a remarkable 230.8% increase in capacitance following 1000 cycles. Wang et al. [83] combined TiO_2 with MoO_3, yielding a TiO_2/MoO_3 composite material. This TiO_2/MoO_3 heterojunction enhances the electrochemical performance of MoO_3. Additionally, TiO_2

nanoparticles affixed on the surface of MoO_3 nanobelts contribute to an enlarged specific surface area, resulting in abundant active sites during electrochemical processes. At a current density of 1 A g^{-1}, the specific capacitance reaches 141 F g^{-1}. A proportion of 77.5% of its specific capacitance is retained even after 2000 cycles. Co_3O_4 usually shows excellent energy storage performance. Chen et al. [84] synthesized Co_3O_4/MoO_3 nanosheets using a hydrothermal method and subsequent treat with air plasma. In 1M KOH electrolytes, a specific capacitance of 141 F g^{-1} is realized at 1 A g^{-1}. Remarkably, at scan rates above 0.2 mV s^{-1}, the ratio of pseudocapacitive behavior is more than 50%. The Co_3O_4/MoO_3 electrode exhibits exceptional cycle stability, retaining 91.4% of capacitance after 1000 cycles at 3 A g^{-1}. Wang et al. [85] constructed a VO_x@MoO_3 composite through a facile electrochemical method. The effective interaction between VO_x and MoO_3 modified the chemical environment and electronic structure, showing enhanced performance. This composite delivers a high capacitance of 1,980 mF cm^{-2} at 2 mA cm^{-2}. The MoO_3 layer can also help to prevent the deformation of the VO_x structure, resulting in 94% of capacitance retention over 10,000 cycles. Muduli et al. [86] synthesized MoO_3@ZnO composite materials using a facile solid-state impregnation–calcination method. The redox behavior of MoO_3 and the porous nature of ZnO facilitated the electrolyte ion interaction into the composite frameworks, which improved the capacitive performance. The MoO_3@ZnO composite shows a specific capacitance of 280 F g^{-1} at 1 A g^{-1}. The composite material shows a power density of 650 W kg^{-1} at an energy density of 65 W h kg^{-1} and is stable over 10,000 cycles at 5 A g^{-1} with 98% capacitance retention. The electrochemical performances of some reported Mo-based materials and metallic oxide composites are presented in Table 4.

Table 4. The electrochemical performances of nanocomposites of Mo-based materials and metallic oxides.

Electrode Material	Method	Structure	Specific Capacitance	Capacitance Retention	Ref.
MoS_2/MnO_2	electrochemical exfoliation	heterojunction	275 F g^{-1} (2 A g^{-1})	89%, 10,000 cycles	[80]
Cr_2O_3-MoO_2	magnetron sputtering	nanosheets	340.8 F g^{-1} (2 mA cm^{-2})	91.7%, 20,000 cycles	[81]
Fe_3O_4-MoO_2	electrodeposition	nanofilms	65 mF cm^{-2} (2 mV s^{-1})	230.8%, 1000 cycles	[82]
TiO_2/MoO_3	hydrothermal	heterojunction	141 F g^{-1} (1 A g^{-1})	77.5%, 2000 cycles	[83]
Co_3O_4/MoO_3	hydrothermal	nanosheets	141 F g^{-1} (1 A g^{-1})	91.4%, 1000 cycles	[84]
VO_x@MoO_3	electrodeposition	nanorods	1980 mF cm^{-2} (2 mA cm^{-2})	94%, 10,000 cycles	[85]
MoO_3@ZnO	solid-state impregnation–calcination	nanoparticles and nanorods	280 F g^{-1} (1 A g^{-1})	98%, 10,000 cycles	[86]

2.3.2. Nanocomposites of Mo-Based Materials and Carbon

The carbon-based materials, such as graphene, carbon nanotube, and porous carbon, show high conductivity and structural stability, which are important in fabricating the electrode materials in supercapacitors [87].

There is a growing trend to combine Mo-based materials with carbon material to fabricate nanocomposite electrodes. This nanocomposite often presents high electrical conductivity and a shortened ion diffusion distance, favoring improved electrochemical performance. Sun et al. [88] synthesized MoO_2@C/CNT through a calcination method. The MoO_2 nanoparticles were distributed uniformly inside the carbon rods, which effectively benefited their electron transportation. The synergy between MoO_2 and CNT results in a remarkable electrochemical performance. A specific capacitance of 1667.2 F g^{-1} was achieved at a current density of 1 A g^{-1} and the capacitance retention reached 92.8% after 3000 cycles at 5 A g^{-1}. Tiwari et al. [89] directly loaded atomically thick hierarchical MoS_2 nanosheets onto carbon nanotubes using magnetron sputtering, fabricating a MoS_2@CNT heterostructure. The MoS_2 nanosheets on the surface of the composite provide sufficient

sites for charge storage. At a scan rate of 5 mV s^{-1}, the specific capacitance reaches 337 mF cm^{-2}. Even after 2500 cycles, the MoS_2@CNT retains 97.6% of its specific capacitance. Beyond the one-dimensional CNT, two-dimensional nanomaterials, for example graphene, combining with Mo-based materials, also exhibit exceptional performance. Tian et al. [90] proposed a microwave-based synthesis strategy for MoP/MoO_2/CNT nanocomposites. The interwoven fibers offer abundant pathways for ion diffusion, thereby enhancing the ion transfer and electrochemical performance of MoP/MoO_2/CNT. The specific capacitance of MoP/MoO_2/CNT at 1 A g^{-1} is 447.6 F g^{-1}, when the capacitance retention is 86.5% even after 10,000 cycles. Furthermore, the MoP/MoO_2/CNT shows an energy density of 31.6 W h kg^{-1} at a power density of 190 W kg^{-1}. Zhao et al. [91] deposited MoS_2 films on graphene aerogel (GA) using a magnetron sputtering process to synthesize a MoS_2/GA composite as a high-performance electrode material for supercapacitors. This synthesis process not only realizes the advantages of GA such as a 3D porous network structure and large surface area, but also achieves the effective interfacial contact between MoS_2 and the graphene sheet at a large scale. At a current density of 0.5 A g^{-1}, the MoS_2/GA electrode exhibits a high specific capacitance of 187.3 F g^{-1}. Additionally, the specific capacitance increases by 93.5% after 1000 cycles at 2 A g^{-1}. Furthermore, doping graphene with heteroatoms can further facilitate rapid electron transport. Liu et al. [92] loaded the flower-like MoS_2 onto the surface of N-doped graphene, producing a MoS_2/N-3DG nanocomposite. At a current density of 0.2 A g^{-1}, the specific capacitance reaches 301.2 F g^{-1}. After 1000 cycles at 1 A g^{-1}, the specific capacitance remains at 82%. As illustrated in Figure 7c, Chen et al. [93] synthesized MoO_2@NPGA nanomaterials using a hydrothermal and calcination method. The synergistic effect between MoO_2 and N, P co-doped graphene aerogel significantly boosts the electrochemical performance of MoO_2@NPGA. The MoO_2@NPGA achieves a high specific capacitance of 335 F g^{-1} at 1 A g^{-1} and the specific capacitance remains 88% after 6000 cycles. The assembled symmetrical supercapacitor device shows a high energy density of 23.75 W h kg^{-1} at a power density of 300 W kg^{-1} and an energy density of 17.1 W h kg^{-1} at a power density of 6005 W kg^{-1}. The electrochemical performances of some reported Mo-based materials and carbon composites are presented in Table 5.

Table 5. The electrochemical performances of nanocomposites of Mo-based materials and carbon.

Electrode Material	Method	Structure	Specific Capacitance	Capacitance Retention	Ref.
MoO_2@C/CNT	calcination	nanorods	1667.2 F g^{-1} (1 A g^{-1})	92.8%, 3000 cycles	[88]
MoS_2/CNT	magnetron sputtering	heterojunction	337 mF cm^{-2} (5 mV s^{-1})	97.6%, 2500 cycles	[89]
MoP/MoO_2/CNT	microwave	nanofibers	447.6 F g^{-1} (1 A g^{-1})	86.5%, 10,000 cycles	[90]
MoS_2/GA	liquid phase exfoliation	nanofilms	175 F g^{-2} (1 A g^{-1})	93.5%, 1000 cycles	[91]
MoS_2/N-3DG	hydrothermal	nanoflowers	301.2 F g^{-1} (0.2 A g^{-1})	82%, 1000 cycles	[92]
MoO_2@NPGA	hydrothermal	porous framework	335 F g^{-1} (1 A g^{-1})	88%, 6000 cycles	[93]

2.3.3. Nanocomposites of Mo-Based Materials and Metallic Sulfides

Metal sulfides are abundant in nature and can form complexes with various metal ions [94]. Notably, researchers have integrated Mo-based materials with metal sulfides, aiming to amplify the electrochemical performance.

Deng et al. [95] synthesized porous MoO_2/MoS_2 nanoblocks using a hydrothermal method. At a current density of 1 A g^{-1}, the MoO_2/MoS_2 exhibited a specific capacitance of 1667.3 F g^{-1}. Even at 10 A g^{-1}, a capacitance retention rate of 94.75% was achieved after 5000 cycles. Similarly, Yang et al. [96] reported a NiMo-O-S nanocomposite with a microsphere structure, as illustrated in Figure 7d. At a current density of 1 A g^{-1}, NiMo-O-S showed a high specific capacitance of 2177.5 F g^{-1}. Even after 5000 cycles, the specific capacitance retained 86.25%. The assembled supercapacitor achieved an energy density of 50.61 W h kg^{-1} at a power density of 850 W kg^{-1} and showed excellent long-term

electrochemical cycle stability, with capacitance retention of 93.38% after 10,000 cycles. Qin et al. [97] synthesized MoS_2/NiS yolk–shell microspheres using a hydrothermal method. Benefitting from the interfacial effect and hollow structure, MoS_2/NiS showed a specific capacitance of 1493 F g^{-1} at 0.2 A g^{-1} and maintained a specific capacitance of 1165 F g^{-1} even at a high current density of 2 A g^{-1}. The asymmetric supercapacitors based on MoS_2/NiS and activated carbon showed an energy density of 31 W h kg^{-1} at a power density of 155.7 W h kg^{-1} and a capacitance retention of about 100% after 10,000 cycles.

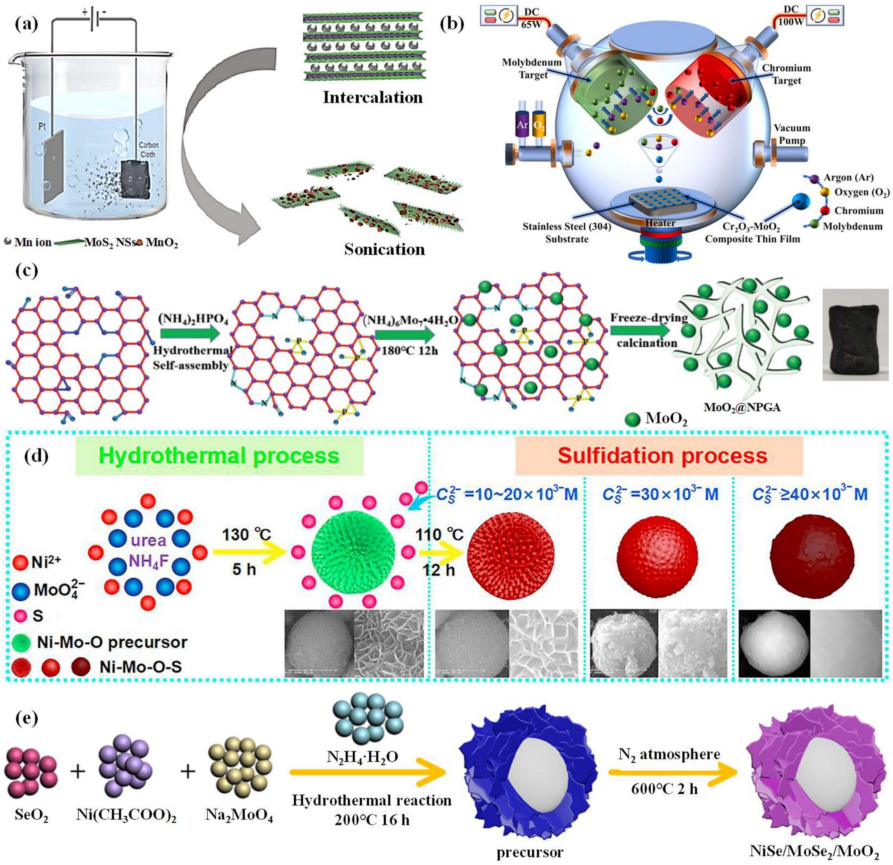

Figure 7. Schematic diagrams of synthesis. (**a**) MoS_2/MnO_2 heterostructure. Reprinted with permission from [80]. Copyright 2022, Elsevier. (**b**) MoS_2@CNT heterostructure. Reprinted with permission from [81]. Copyright 2021, Elsevier. (**c**) MoO_2@NPGA. Reprinted with permission from [93]. Copyright 2020, Canadian Science Publishing. (**d**) NiMo-O-S nanospheres. Reprinted with permission from [96]. Copyright 2019, Elsevier. (**e**) NiSe/$MoSe_2$/MoO_2. Reprinted with permission from [98]. Copyright 2020, Elsevier.

As illustrated in Figure 7e, Liu et al. [98] synthesized NiSe/$MoSe_2$/MoO_2 nanocomposites with a hierarchical hollow structure using an annealing process. This structure increases the contact area between the active material and the electrolyte, thereby shortening the path of electrolyte ion transport. The NiSe/$MoSe_2$/MoO_2 showed a specific capacitance of 1061 F g^{-1} at 2 A g^{-1}, while preserving 57% of the initial capacitance at 20 A g^{-1} and retaining 93.9% of the initial capacitance at 3 A g^{-1} after 10,000 cycles. Furthermore, the NiSe/$MoSe_2$/MoO_2//AC supercapacitor showed remarkable energy density of 48.1 W h kg^{-1} at a power density of 428 W h kg^{-1} and maintained 20.4 W h kg^{-1} even at a high power density of 7.3 kW kg^{-1}. Wang et al. [99] reported the nanowire-like $NiMoO_4$/$NiSe_2$/$MoSe_2$ composite through in situ selenization. The $NiMoO_4$/$NiSe_2$/$MoSe_2$ showed heterogeneous interfaces, abundant defects, and excellent electrical conductivity. At a scan rate of 5 mV s^{-1}, $NiMoO_4$/$NiSe_2$/$MoSe_2$ displayed a specific capacitance of 1020 F g^{-1} and maintained a capacitance retention of 86.1% after 5000 cycles at 10 A g^{-1}. Krishna et al. [100] explored the MSe/Mo_3Se_4 (M: Zn, Mn, Ni)

nanocomposites using a hydrothermal method. Among these materials, the $NiSe/Mo_3Se_4$ nanosheets, with a hierarchical porous and unique interconnected structure, showed superior electrochemical performance. A specific capacitance of 252 mA h g^{-1} was achieved at 1 A g^{-1}. The capacitance retention is 80% after 80,000 cycles at a high current density of 15 mA cm^{-2} and the corresponding coulombic efficiency is 99%. The electrochemical performances of some reported Mo-based materials and metallic sulfides composites are presented in Table 6.

Table 6. The electrochemical performances of nanocomposites of Mo-based materials and metallic sulfides.

Electrode Material	Method	Structure	Specific Capacitance	Capacitance Retention	Ref.
MoO_2/MoS_2	hydrothermal	nanoblocks	1667.3 F g^{-1} (1 A g^{-1})	94.75%, 5000 cycles	[95]
NiMo-O-S	calcination	nanospheres	2177.5 F g^{-1} (1 A g^{-1})	86.25%, 5000 cycles	[96]
MoS_2/NiS	hydrothermal	yolk–shell microspheres	1165 F g^{-1} (2 A g^{-1})	~100%, 10,000 cycles	[97]
$NiSe/MoSe_2/MoO_2$	growth-annealing	hierarchical hollow	1061 F g^{-1} (2 A g^{-1})	93.9%, 10,000 cycles	[98]
$NiMoO_4/NiSe_2/MoSe_2$	hydrothermal	nanowires	1020 F g^{-1} (5 mV s^{-1})	86.1%, 5000 cycles	[99]
$ZnSe/Mo_3Se_4$		micro solid spheres	96 mA h g^{-1} (1 A g^{-1})	N/A	
$MnSe/Mo_3Se_4$	hydrothermal	micro block sheets	118 mA h g^{-1} (1 A g^{-1})	N/A	[100]
$NiSe/Mo_3Se_4$		nanosheet spheres	252 mA h g^{-1} (1 A g^{-1})	80%, 80,000 cycles	

(N/A = unavailable).

2.4. Mo-Based MOFs and Mo-Based Materials Deriving from MOFs

Metal–organic frameworks (MOFs), composed of central metal ions and organic ligands, possess adjustable morphology, high specific surface area, and porous nanostructure. MOFs show widespread applications in energy storage fields, such as supercapacitors, sodium-ion batteries, lithium-ion batteries, and photocatalysis, etc. [101]. In recent years, researchers have made efforts to enhance the electrochemical capabilities of Mo-based MOFs and Mo-based materials deriving from MOFs.

Zhang et al. [102] combined a Mo-based metal–organic framework with polyaniline (Mo-MOF/PANI) through an in situ polymerization process. This Mo-MOF/PANI nanocomposite possesses high specific surface area, which enhances the interfacial dynamics and accelerates the transfer of charges. At a current density of 5 mA g^{-1}, the specific capacitance reaches 110 F g^{-1}. However, single-metal MOF materials show poor conductivity. Consequently, researchers have devoted themselves to fabricating MOF materials with dual-metal sites to enhance performance through synergistic effects. Cai et al. [103] manufactured a dandelion-like needle-shaped bimetallic MOF (BiMo-MOF) on nickel foam using an electrodeposition technique. This unique structure facilitates the rapid movement of electrolyte ions within the bimetallic MOF channel. The BiMo-MOF achieved a specific capacitance of 864 F g^{-1} at 10 A g^{-1}, retained 43% of its capacitance even at 100 A g^{-1}, and maintained a capacitance retention of 81.2% after 8000 cycles at 50 A g^{-1}. Li et al. [104] developed Mo-Ni-MOF nanocomposites (Figure 8a), wherein the arrangement of stacked nanorods results in enlarged channels. The Mo-Ni-MOF shows a specific capacitance of 802 C g^{-1} at 1 A g^{-1}. Additionally, Mo-Ni-MOF shows an energy density of 59 W h kg^{-1} at a power density of 802 W kg^{-1}, alongside a retention rate of 93% over 20,000 cycles (Figure 8b).

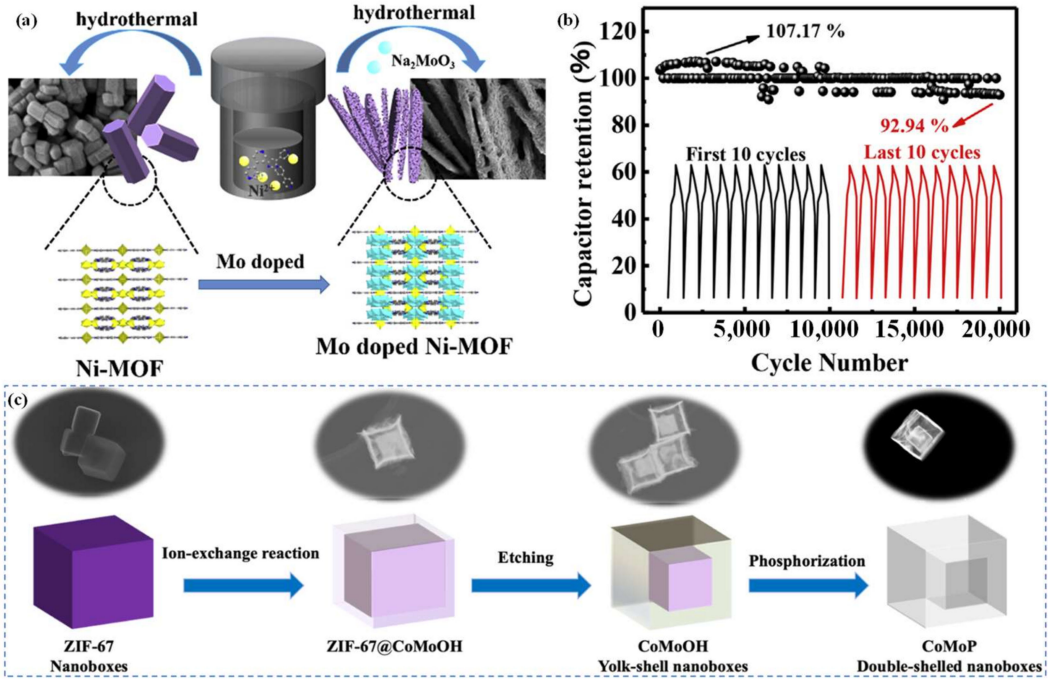

Figure 8. (**a**) Schematic diagram of the synthesis of Mo doped Ni-MOF nanosheets; (**b**) cyclic performance of Mo doped Ni-MOF//AC at 5 A g^{-1}. Reprinted with permission from [104]. Copyright 2020, Elsevier. (**c**) Schematic diagram of the synthesis of CoMoP double-shelled nanoboxes. Reprinted with permission from [105]. Copyright 2021, open access.

Beyond Mo-based materials and MOF composites, MOF derivatives also show potential as alternative composite materials in supercapacitors. By converting MOFs into derived materials such as carbonaceous substances or metal compounds with pronounced porosity, their energy storage performance can be significantly enhanced. Govindan et al. [106] reported a nanocomposite of CeO_2/C and MoS_2 deriving from MOF (CeO_2/C/MoS_2), which showed a high specific surface area of 32.767 m^2 g^{-1}, a specific capacitance of 1325.67 F g^{-1} at 1 A g^{-1}, and a capacitance retention of 92.8% after 1000 cycles. The CeO_2/C/MoS_2 achieves an energy density of 34.55 W h kg^{-1} at a power density of 666.7 W kg^{-1}. Safartoobi et al. [107] prepared Ag_2MoO_4 nanoparticles based on AgMo-MOF, featuring a specific surface area of 56.58 m^2 g^{-1} and a specific capacitance of 1468.7 F g^{-1} at a current density of 1 A g^{-1}, with a capacitance retention of 90%. When the power density reaches 1123.6 W kg^{-1}, the energy density reaches 72.1 W h kg^{-1}. The capacitance retention remains 88% after 5000 cycles. Similarly, Gourji et al. [105] synthesized double-shell hollow cobalt–molybdenum phosphide nanoboxes (CoMoP-DSHNBs) using ZIF-67 as a template, as shown in Figure 8c. CoMoP-DSHNBs possesses numerous pore structures. In the three-electrode system, CoMoP-DSHNBs demonstrates a specific capacitance of 1204 F g^{-1} at 1 A g^{-1}, maintaining 87% of the initial capacitance after 20,000 cycles. The CoMoP-DSHNBs//AC supercapacitor shows a high specific energy density of 49.99 W h kg^{-1} and a maximum power density of 7539.41 W kg^{-1}. The capacitance retention reaches 84.5% of the initial capacitance after 20,000 cycles. The electrochemical performances of some reported Mo-based MOF materials are presented in Table 7.

Table 7. The electrochemical performances of Mo-based MOF materials.

Electrode Material	Method	Structure	Specific Capacitance	Capacitance Retention	Ref.
Mo-MOF/PANI	solution method	nanorod bundles	110 F g^{-1} (5 mA g^{-1})	N/A	[102]
BiMo-MOF	electrodeposition	dandelion-like	864 F g^{-1} (10 A g^{-1})	81.2%, 8000 cycles	[103]
Mo-Ni-MOF	hydrothermal	nanosheets	802 C g^{-1} (1 A g^{-1})	93%, 20,000 cycles	[104]
$CeO_2/C/MoS_2$	MOF-derived	nanoparticles	1325.67 F g^{-1} (1 A g^{-1})	92.8%, 1000 cycles	[106]
Ag_2MoO_4	MOF-derived	nanoparticles	1468.7 F g^{-1} (1 A g^{-1})	90%, 5000 cycles	[107]
CoMoP-DSHNBs	MOF-derived	hollow nanoboxes	1204 F g^{-1} (1 A g^{-1})	87%, 20,000 cycles	[105]

(N/A = unavailable).

3. Conclusions and Outlook

The supercapacitor, as a novel energy storage device, plays a vital role in solving the energy crisis. In comparison to the traditional dielectric capacitors, supercapacitors offer several orders of magnitude higher energy density. Compared with the traditional batteries, supercapacitors facilitate rapid charge and discharge processes, thereby exhibiting higher power density. The above-mentioned characteristics significantly widen their applications in energy storage fields. In supercapacitors, electrode materials play a pivotal factor in electrochemical performance. Consequently, the research and development of high-performance electrode materials is important in improving the performance of supercapacitors.

Mo-based electrode materials have attracted much attention due to their abundant resources, simple preparation process, and high theoretical capacitance. This review presents an overview of Mo-based electrode materials in supercapacitors, including: (1) binary Mo-based electrode materials; (2) ternary Mo-based electrode materials; (3) nanocomposites of Mo-based electrode materials; and (4) Mo-based MOFs and derivative materials. Although there has been significant progress in the development of Mo-based electrode materials in supercapacitors, there are still some problems to solve.

(1) Conductivity and electrochemical stability: The optimized Mo-based electrode materials should possess high conductivity and excellent electrochemical stability to facilitate improved performance and long cycling life.
(2) The excellent electrode materials should present a high specific surface area and a hierarchical porous structure to facilitate fast ion transport.
(3) Cost of mass-industrial manufacture: The cost of mass-industrial manufacture for Mo-based materials is still a challenge, which should be further improved in the application of supercapacitors.
(4) Research on the energy storage mechanism: The energy storage mechanism in supercapacitors remain controversial. Therefore, it is essential to make efforts in investigating the energy storage mechanism.
(5) Application of computational materials science: It is important to resort to computational materials science to design and exploit novel Mo-based electrode materials. In addition, this approach can decrease experimental costs and accelerate experimental processes through a large number of parallel experiments.
(6) There are limited reports on Mo-based MXene materials. It is necessary to etch various MAX phases to develop a series of Mo-based MXenes and explore their application in supercapacitors.

Author Contributions: Conceptualization, writing—original draft preparation, Y.W.; methodology and data curation, H.W.; writing—review and supervision, G.Q. All authors have read and agreed to the published version of the manuscript.

Funding: This work was funded by the National Natural Science Foundation of China (22109140), Key Scientific and Technological Project of Henan Province (222102240082), China Postdoctoral

Science Foundation (2022M722866), International Talent Cooperation Program in Henan Province (HNGD2022036), and the Postdoctoral Science Foundation of Zhengzhou University (22120030).

Data Availability Statement: Data sharing is not applicable to this article.

Conflicts of Interest: The authors declare no conflict of interest.

References

1. Song, D.; Liu, Y.; Qin, T.; Gu, H.; Cao, Y.; Shi, H. Overview of the policy instruments for renewable energy development in China. *Energies* **2022**, *15*, 6513. [CrossRef]
2. Pan, Y.; Dong, F. Dynamic evolution and driving factors of new energy development: Fresh evidence from China. *Technol. Forecast. Soc. Chang.* **2022**, *176*, 14. [CrossRef]
3. Guo, L.; Hu, P.; Wei, H. Development of supercapacitor hybrid electric vehicle. *J. Energy Storage* **2023**, *65*, 8. [CrossRef]
4. Lamba, P.; Singh, P.; Singh, P.; Singh, P.; Bharti; Kumar, A.; Gupta, M.; Kumar, Y. Recent advancements in supercapacitors based on different electrode materials: Classifications, synthesis methods and comparative performance. *J. Energy Storage* **2022**, *48*, 103871. [CrossRef]
5. Frackowiak, E.; Abbas, Q.; Béguin, F. Carbon/carbon supercapacitors. *J. Energy Chem.* **2013**, *22*, 226–240. [CrossRef]
6. Conway, B.E. Transition from "supercapacitor" to "battery" behavior in electrochemical energy storage. *J. Electrochem. Soc.* **1991**, *138*, 1539–1548. [CrossRef]
7. Ji, H.; Zhao, X.; Qiao, Z.; Jung, J.; Zhu, Y.; Lu, Y.; Zhang, L.L.; MacDonald, A.H.; Ruoff, R.S. Capacitance of carbon-based electrical double-layer capacitors. *Nat. Commun.* **2014**, *5*, 3317. [CrossRef] [PubMed]
8. Lu, X.F.; Wang, A.L.; Xu, H.; He, X.J.; Tong, Y.X.; Li, G.R. High-performance supercapacitors based on MnO_2 tube-in-tube arrays. *J. Mater. Chem. A* **2015**, *3*, 16560–16566. [CrossRef]
9. Sharma, S.; Chand, P. Supercapacitor and electrochemical techniques: A brief review. *Results Chem.* **2023**, *5*, 100885. [CrossRef]
10. Kumar, S.; Saeed, G.; Zhu, L.; Hui, K.N.; Kim, N.H.; Lee, J.H. 0D to 3D carbon-based networks combined with pseudocapacitive electrode material for high energy density supercapacitor: A review. *Chem. Eng. J.* **2021**, *403*, 126352. [CrossRef]
11. Wang, D.; Tang, K.; Xiao, J.; Li, X.; Long, M.; Chen, J.; Gao, H.; Chen, W.; Liu, C.; Liu, H. Advances of electrospun Mo-based nanocomposite fibers as anode materials for supercapacitors. *Sustain. Mater. Technol.* **2021**, *29*, e00302. [CrossRef]
12. Xiong, C.; Zhang, Y.; Xu, J.; Dang, W.; Sun, X.; An, M.; Ni, Y.; Mao, J. Kinetics process for structure-engineered integrated gradient porous paper-based supercapacitors with boosted electrochemical performance. *Nano Res.* **2023**, *16*, 9471–9479. [CrossRef]
13. Xiong, C.; Zheng, C.; Jiang, X.; Xiao, X.; Wei, H.; Zhou, Q.; Ni, Y. Recent progress of green biomass based composite materials applied in supercapacitors, sensors, and electrocatalysis. *J. Energy Storage* **2023**, *72*, 108633. [CrossRef]
14. Xiong, C.; Wang, T.; Han, J.; Zhang, Z.; Ni, Y. Recent research progress of paper-based supercapacitors based on cellulose. *Energy Environ. Mater.* **2023**, e12651. [CrossRef]
15. Mendoza-Sánchez, B.; Brousse, T.; Ramirez Castro, C.; Nicolosi, V.; Grant, P.S. An investigation of nanostructured thin film α-MoO_3 based supercapacitor electrodes in an aqueous electrolyte. *Electrochim. Acta* **2013**, *91*, 253–260. [CrossRef]
16. Ma, H.; Liang, J.; Qiu, J.; Jiang, L.; Ma, L.; Sheng, H.; Shao, M.; Wang, Q.; Li, F.; Fu, Y.; et al. A biocompatible supercapacitor diode with enhanced rectification capability toward ion/electron-coupling logic operations. *Adv. Mater.* **2023**, *35*, e2301218. [CrossRef] [PubMed]
17. Vikraman, D.; Hussain, S.; Karuppasamy, K.; Santhoshkumar, P.; Kathalingam, A.; Jung, J.; Kim, H.S. Fabrication of asymmetric supercapacitors using molybdenum dichalcogenide nanoarray structures. *Int. J. Energy Res.* **2022**, *46*, 18410–18425. [CrossRef]
18. Yuksel, R.; Coskun, S.; Unalan, H.E. Coaxial silver nanowire network core molybdenum oxide shell supercapacitor electrodes. *Electrochim. Acta* **2016**, *193*, 39–44. [CrossRef]
19. Saji, V.S.; Lee, C.W. Molybdenum, molybdenum oxides, and their electrochemistry. *ChemSusChem* **2012**, *5*, 1146–1161. [CrossRef]
20. Mai, L.Q.; Hu, B.; Chen, W.; Qi, Y.Y.; Lao, C.S.; Yang, R.S.; Dai, Y.; Wang, Z.L. Lithiated MoO_3 nanobelts with greatly improved performance for lithium batteries. *Adv. Mater.* **2007**, *19*, 3712–3716. [CrossRef]
21. De Castro, I.A.; Datta, R.S.; Ou, J.Z.; Castellanos Gomez, A.; Sriram, S.; Daeneke, T.; Kalantar-Zadeh, K. Molybdenum oxides—From fundamentals to functionality. *Adv. Mater.* **2017**, *29*, 31. [CrossRef] [PubMed]
22. Huang, C.; Zhang, W.; Zheng, W. The debut and spreading the landscape for excellent vacancies-promoted electrochemical energy storage of nano-architected molybdenum oxides. *Mater. Today Energy* **2022**, *30*, 101154. [CrossRef]
23. Pan, W.; Tian, R.; Jin, H.; Guo, Y.; Zhang, L.; Wu, X.; Zhang, L.; Han, Z.; Liu, G.; Li, J.; et al. Structure, optical, and catalytic properties of novel hexagonal metastable h-MoO_3 nano- and microrods synthesized with modified liquid-phase processes. *Chem. Mater.* **2010**, *22*, 6202–6208. [CrossRef]
24. Prakash, N.G.; Dhananjaya, M.; Narayana, A.L.; Shaik, D.P.M.D.; Rosaiah, P.; Hussain, O.M. High performance one dimensional α-MoO_3 nanorods for supercapacitor applications. *Ceram. Int.* **2018**, *44*, 9967–9975. [CrossRef]
25. Niu, Y.; Li, X.; Su, H.; Li, J.; Qi, Y. Formation of three dimensional porous h-MoO_3 architecture and its application in supercapacitors. *Mater. Lett.* **2022**, *316*, 132062. [CrossRef]
26. Zhu, Y.; Tan, Y.; Li, H. MoO_3 nanoplates preparation via self-sacrifice C_3N_4 for supercapacitors in an acid electrolyte. *J. Energy Storage* **2023**, *60*, 106657. [CrossRef]

27. Hao, J.; Zhang, J.; Xia, G.; Liu, Y.; Zheng, Y.; Zhang, W.; Tang, Y.; Pang, W.K.; Guo, Z. Heterostructure manipulation via in situ localized phase transformation for high-rate and highly durable lithium ion storage. *ACS Nano* **2018**, *12*, 10430–10438. [CrossRef]
28. Ma, B.; Hao, W.; Ruan, W.; Yuan, C.; Wang, Q.; Teng, F. Unveiling capacitive behaviors of MoO_2 in different electrolytes and flexible MoO_2-based asymmetric micro-supercapacitor. *J. Energy Storage* **2022**, *52*, 104833. [CrossRef]
29. Wu, K.; Zhao, J.; Zhang, X.; Zhou, H.; Wu, M. Hierarchical mesoporous MoO_2 sphere as highly effective supercapacitor electrode. *J. Taiwan Inst. Chem. Eng.* **2019**, *102*, 212–217. [CrossRef]
30. Zhao, X.; Wang, H.E.; Cao, J.; Cai, W.; Sui, J. Amorphous/crystalline hybrid MoO_2 nanosheets for high-energy lithium-ion capacitors. *Chem. Commun.* **2017**, *53*, 10723–10726. [CrossRef]
31. Luo, Z.; Miao, R.; Huan, T.D.; Mosa, I.M.; Poyraz, A.S.; Zhong, W.; Cloud, J.E.; Kriz, D.A.; Thanneeru, S.; He, J.; et al. Mesoporous MoO_{3-x} material as an mfficient mlectrocatalyst for hydrogen evolution reactions. *Adv. Energy Mater.* **2016**, *6*, 11. [CrossRef]
32. Gurusamy, L.; Karuppasamy, L.; Anandan, S.; Liu, N.; Lee, G.J.; Liu, C.H.; Wu, J.J. Enhanced performance of charge storage supercapattery by dominant oxygen deficiency in crystal defects of 2-D MoO_{3-x} nanoplates. *Appl. Surf. Sci.* **2021**, *541*, 148676. [CrossRef]
33. Kuwahara, Y.; Furuichi, N.; Seki, H.; Yamashita, H. One-pot synthesis of molybdenum oxide nanoparticles encapsulated in hollow silica spheres: An efficient and reusable catalyst for epoxidation of olefins. *J. Mater. Chem. A* **2017**, *5*, 18518–18526. [CrossRef]
34. Li, X.; Wang, D.; Zhang, Y.; Liu, L.; Wang, W. Surface-ligand protected reduction on plasmonic tuning of one-dimensional MoO_{3-x} nanobelts for solar steam generation. *Nano Res.* **2020**, *13*, 3025–3032. [CrossRef]
35. Wu, Q.L.; Zhao, S.X.; Yu, L.; Zheng, X.X.; Wang, Y.F.; Yu, L.Q.; Nan, C.W.; Cao, G.Z. Oxygen vacancy-enriched MoO_{3-x} nanobelts for asymmetric supercapacitors with excellent room/low temperature performance. *J. Mater. Chem. A* **2019**, *7*, 13205–13214. [CrossRef]
36. Cong, S.; Hadipour, A.; Sugahara, T.; Wei, T.; Jiu, J.; Ranjbar, S.; Hirose, Y.; Karakawa, M.; Nagao, S.; Aernouts, T.; et al. Modifying the valence state of molybdenum in the efficient oxide buffer layer of organic solar cells via a mild hydrogen peroxide treatment. *J. Mater. Chem. C* **2017**, *5*, 889–895. [CrossRef]
37. Bai, Y.; Ma, Y.; Zheng, S.; Zhang, C.; Hu, C.; Liang, B.; Xu, Y.; Huang, G.; Yang, R. Oxygen deficiency and single-crystalline MoO_{3-x} nanobelt as advanced supercapacitor negative electrode and dye adsorbent. *Colloids Surf. A* **2022**, *647*, 129064. [CrossRef]
38. Salkar, A.V.; Naik, A.P.; Peña, G.D.J.G.; Bharath, G.; Haija, M.A.; Banat, F.; Morajkar, P.P. 2D α-MoO_{3-x} truncated microplates and microdisks as electroactive materials for highly efficient asymmetric supercapacitors. *J. Energy Storage* **2022**, *48*, 103958. [CrossRef]
39. Cao, Y.B.; Zhi, S.X.; Qi, H.B.; Zhang, Y.; Qin, C.; Yang, S.P. Evolution behavior of ex-situ NbC and properties of Fe-based laser clad coating. *Opt. Laser Technol.* **2020**, *124*, 8. [CrossRef]
40. Gao, J.; Xu, C.; Tian, X.; Sun, M.; Zhao, J.; Ma, J.Y.; Zhou, H.; Xiao, J.; Wu, M. Design bifunctional vanadium carbide embedded in mesoporous carbon electrode for supercapacitor and dye-sensitized solar cell. *Sol. Energy* **2020**, *206*, 848–854. [CrossRef]
41. Wan, C.; Zhang, R.; Wang, S.; Liu, X. Molten salt electrolytic fabrication of TiC-CDC and its applications for supercapacitor. *J. Mater. Sci. Technol.* **2017**, *33*, 788–792. [CrossRef]
42. Xu, Y.; Yang, Q.Q.; Zhang, W.B.; Liu, M.C.; Kong, L.B. Enhanced performance for a high electrical conductive Mo_2C electrode based proton ionic liquid electrolytes in supercapacitors. *Mater. Res. Express* **2018**, *5*, 75508. [CrossRef]
43. Yu, Y.; Guo, Z.; Peng, Q.; Zhou, J.; Sun, Z. Novel two-dimensional molybdenum carbides as high capacity anodes for lithium/sodium-ion batteries. *J. Mater. Chem. A* **2019**, *7*, 12145–12153. [CrossRef]
44. Luo, Q.; Lu, C.; Liu, L.; Zhu, M. A review on the synthesis of transition metal nitride nanostructures and their energy related applications. *Green Energy Environ.* **2023**, *8*, 406–437. [CrossRef]
45. Xiao, X.; Yu, H.; Jin, H.; Wu, M.; Fang, Y.; Sun, J.; Hu, Z.; Li, T.; Wu, J.; Huang, L.; et al. Salt-templated synthesis of 2D metallic MoN and other nitrides. *ACS Nano* **2017**, *11*, 2180–2186. [CrossRef] [PubMed]
46. Gao, Z.; Zhang, T.; Wang, Q.; Heinz Mayrhofer, P. Nanostructured zig-zag γ-Mo_2N thin films produced by glancing angle deposition for flexible symmetrical solid-state supercapacitors. *Mater. Des.* **2023**, *225*, 111432. [CrossRef]
47. Djire, A.; Siegel, J.B.; Ajenifujah, O.; He, L.; Thompson, L.T. Pseudocapacitive storage via micropores in high-surface area molybdenum nitrides. *Nano Energy* **2018**, *51*, 122–127. [CrossRef]
48. Wang, L.; Liu, X.; Luo, J.; Duan, X.; Crittenden, J.; Liu, C.; Zhang, S.; Pei, Y.; Zeng, Y.; Duan, X. Self-Optimization of the Active Site of Molybdenum Disulfide by an Irreversible Phase Transition during Photocatalytic Hydrogen Evolution. *Angew. Chem. Int. Ed.* **2017**, *56*, 7610–7614. [CrossRef]
49. Li, R.; Liang, S.; Aihemaiti, A.; Li, S.; Zhang, Z. Effectively enhanced piezocatalytic activity in flower-like 2H-MoS_2 with tunable S vacancy towards organic pollutant degradation. *Appl. Surf. Sci.* **2023**, *631*, 157461. [CrossRef]
50. Marinov, A.D.; Bravo Priegue, L.; Shah, A.R.; Miller, T.S.; Howard, C.A.; Hinds, G.; Shearing, P.R.; Cullen, P.L.; Brett, D.J.L. Ex situ characterization of 1T/2H MoS_2 and their carbon composites for energy applications, a review. *ACS Nano* **2023**, *17*, 5163–5186. [CrossRef]
51. Li, H.; Han, X.; Jiang, S.; Zhang, L.; Ma, W.; Ma, R.; Zhou, Z. Controllable fabrication and structure evolution of hierarchical 1T-MoS_2 nanospheres for efficient hydrogen evolution. *Green Energy Environ.* **2022**, *7*, 314–323. [CrossRef]
52. Liu, X.; Liu, L.; Wu, Y.; Wang, Y.; Yang, J.; Wang, Z. Rosette-like MoS_2 nanoflowers as highly active and stable electrodes for hydrogen evolution reactions and supercapacitors. *RSC Adv.* **2019**, *9*, 13820–13828. [CrossRef] [PubMed]
53. Teli, A.M.; Beknalkar, S.A.; Mane, S.M.; Bhat, T.S.; Kamble, B.B.; Patil, S.B.; Sadale, S.B.; Shin, J.C. Electrodeposited crumpled MoS_2 nanoflakes for asymmetric supercapacitor. *Ceram. Int.* **2022**, *48*, 29002–29010. [CrossRef]

54. Joseph, N.; Muhammed Shafi, P.; Chandra Bose, A. Metallic 1T-MoS_2 with defect induced additional active edges for high performance supercapacitor application. *N. J. Chem.* **2018**, *42*, 12082–12090. [CrossRef]
55. Gupta, H.; Chakrabarti, S.; Mothkuri, S.; Padya, B.; Rao, T.N.; Jain, P.K. High performance supercapacitor based on 2D-MoS_2 nanostructures. *Mater. Today Proc.* **2020**, *26*, 20–24. [CrossRef]
56. Vattikuti, S.V.P.; Devarayapalli, K.C.; Nagajyothi, P.C.; Shim, J. Microwave synthesized dry leaf-like mesoporous $MoSe_2$ nanostructure as an efficient catalyst for enhanced hydrogen evolution and supercapacitor applications. *Microchem. J.* **2020**, *153*, 104446. [CrossRef]
57. Upadhyay, S.; Pandey, O.P. Synthesis of layered 2H-$MoSe_2$ nanosheets for the high-performance supercapacitor electrode material. *J. Alloys Compd.* **2021**, *857*, 157522. [CrossRef]
58. Zhang, H.-J.; Wang, Y.-K.; Kong, L.-B. A facile strategy for the synthesis of three-dimensional heterostructure self-assembled $MoSe_2$ nanosheets and their application as an anode for high-energy lithium-ion hybrid capacitors. *Nanoscale* **2019**, *11*, 7263–7276. [CrossRef]
59. Sha, R.; Maity, P.C.; Rajaji, U.; Liu, T.-Y.; Bhattacharyya, T.K. Review—$MoSe_2$ nanostructures and related electrodes for advanced supercapacitor developments. *J. Electrochem. Soc.* **2022**, *169*, 13503. [CrossRef]
60. Zhang, L.; Zheng, S.; Wang, L.; Tang, H.; Xue, H.; Wang, G.; Pang, H. Fabrication of metal molybdate micro/nanomaterials for electrochemical energy storage. *Small* **2017**, *13*, 19. [CrossRef]
61. Yang, J.; Yao, G.; Sun, S.; Chen, Z.; Yuan, S.; Wu, K.; Fu, X.; Wang, Q.; Cui, W. Structural, magnetic properties of in-plane chemically ordered $(Mo_{2/3}R)_2AlC$ (R=Gd, Tb, Dy, Ho, Er and Y) MAX phase and enhanced capacitance of $Mo_{1.33}C$ MXene derivatives. *Carbon* **2021**, *179*, 104–110. [CrossRef]
62. Farahpour, M.; Arvand, M. Single-pot hydrothermal synthesis of copper molybdate nanosheet arrays as electrode materials for high areal-capacitance supercapacitor. *J. Energy Storage* **2021**, *40*, 102742. [CrossRef]
63. Gurusamy, H.; Sivasubramanian, R.; Johnbosco, Y.; Bhagavathiachari, M. Morphology-controlled synthesis of one-dimensional zinc molybdate nanorods for high-performance pseudocapacitor electrode application. *Chem. Pap.* **2020**, *75*, 1715–1726. [CrossRef]
64. Yesuraj, J.; Austin Suthanthiraraj, S.; Padmaraj, O. Synthesis, characterization and electrochemical performance of DNA-templated Bi_2MoO_6 nanoplates for supercapacitor applications. *Mater. Sci. Semicond. Process.* **2019**, *90*, 225–235. [CrossRef]
65. Qu, G.; Li, T.; Jia, S.; Zheng, H.; Li, L.; Cao, F.; Wang, H.; Ma, W.; Tang, Y.; Wang, J. Rapid and scalable synthesis of Mo-based binary and ternary oxides for electrochemical applications. *Adv. Funct. Mater.* **2017**, *27*, 1700928. [CrossRef]
66. Sheng, R.; Hu, J.; Lu, X.; Jia, W.; Xie, J.; Cao, Y. Solid-state synthesis and superior electrochemical performance of $MnMoO_4$ nanorods for asymmetric supercapacitor. *Ceram. Int.* **2021**, *47*, 16316–16323. [CrossRef]
67. Sakthikumar, K.; Ede, S.R.; Mishra, S.; Kundu, S. Shape-selective synthesis of $Sn(MoO_4)_2$ nanomaterials for catalysis and supercapacitor applications. *Dalton Trans.* **2016**, *45*, 8897–8915. [CrossRef]
68. Li, L.; Zhou, J.; Zhang, Y.; Pei, X. Synthesis process optimization and electrochemical properties of $CoMoO_4$ supercapacitor prepared by in situ growth method. *J. Mater. Sci. Mater. Electron.* **2022**, *33*, 23851–23866. [CrossRef]
69. Liang, C.; Meng, Y.; Zhang, Y.; Zhang, H.; Wang, W.; Lu, M.; Wang, G. Insights into the impact of interlayer spacing on MXene-based electrodes for supercapacitors: A review. *J. Energy Storage* **2023**, *65*, 20. [CrossRef]
70. Garg, R.; Agarwal, A.; Agarwal, M. A review on MXene for energy storage application: Effect of interlayer distance. *Mater. Res. Express* **2020**, *7*, 21. [CrossRef]
71. Halim, J.; Kota, S.; Lukatskaya, M.R.; Naguib, M.; Zhao, M.Q.; Moon, E.J.; Pitock, J.; Nanda, J.; May, S.J.; Gogotsi, Y.; et al. Synthesis and characterization of 2D molybdenum carbide (MXene). *Adv. Funct. Mater.* **2016**, *26*, 3118–3127. [CrossRef]
72. Das, M.; Ghosh, S. Theoretical investigation of capacitances in functionalised MXene supercapacitors $M_{n+1}CnO_2$, M. = Ti, V., Nb, Mo. *J. Phys. D Appl. Phys.* **2021**, *55*, 85502. [CrossRef]
73. Zheng, W.; Halim, J.; Persson, P.O.Å.; Rosen, J.; Barsoum, M.W. Effect of vacancies on the electrochemical behavior of Mo-based MXenes in aqueous supercapacitors. *J. Power Sources* **2022**, *525*, 231064. [CrossRef]
74. VahidMohammadi, A.; Mojtabavi, M.; Caffrey, N.M.; Wanunu, M.; Beidaghi, M. Assembling 2D MXenes into highly stable pseudocapacitive electrodes with high power and energy densities. *Adv. Mater.* **2019**, *31*, 1806931. [CrossRef]
75. Li, H.; Hou, Y.; Wang, F.; Lohe, M.R.; Zhuang, X.; Niu, L.; Feng, X. Flexible all-solid-state supercapacitors with high volumetric capacitances boosted by solution processable MXene and electrochemically exfoliated graphene. *Adv. Energy Mater.* **2017**, *7*, 1601847. [CrossRef]
76. Halim, J.; Moon, E.J.; Eklund, P.; Rosen, J.; Barsoum, M.W.; Ouisse, T. Variable range hopping and thermally activated transport in molybdenum-based MXenes. *Phys. Rev. B* **2018**, *98*, 104202. [CrossRef]
77. Zheng, W.; Halim, J.; Rosen, J.; Barsoum, M.W. Aqueous electrolytes, MXene-based supercapacitors and their self-discharge. *Adv. Energy Sustain. Res.* **2022**, *3*, 202100147. [CrossRef]
78. Qin, L.; Tao, Q.; El Ghazaly, A.; Fernandez-Rodriguez, J.; Persson, P.O.Å.; Rosen, J.; Zhang, F. High-Performance ultrathin flexible solid-state supercapacitors based on solution processable $Mo_{1.33}C$ MXene and PEDOT:PSS. *Adv. Funct. Mater.* **2018**, *28*, 1703808. [CrossRef]
79. Qin, L.; Tao, Q.; Liu, X.; Fahlman, M.; Halim, J.; Persson, P.O.Å.; Rosen, J.; Zhang, F. Polymer-MXene composite films formed by MXene-facilitated electrochemical polymerization for flexible solid-state microsupercapacitors. *Nano Energy* **2019**, *60*, 734–742. [CrossRef]

80. Hu, R.; Liao, Y.; Qiao, H.; Li, J.; Wang, K.; Huang, Z.; Qi, X. Electrochemical method integrating exfoliation and in-situ growth to synthesize MoS_2 nanosheets/MnO_2 heterojunction for performance-enhanced supercapacitor. *Ceram. Int.* **2022**, *48*, 23498–23503. [CrossRef]
81. Sharma, M.; Adalati, R.; Kumar, A.; Chawla, V.; Chandra, R. Single step fabrication of nanostructured Cr_2O_3-MoO_2 composite flexible electrode for top-notch asymmetric supercapacitor. *Appl. Surf. Sci.* **2021**, *555*, 149721. [CrossRef]
82. Li, R.; Ba, X.; Wang, Y.; Zuo, W.; Wang, C.; Li, Y.; Liu, J. Direct growth of Fe_3O_4-MoO_2 hybrid nanofilm anode with enhanced electrochemical performance in neutral aqueous electrolyte. *Prog. Nat. Sci. Mater. Int.* **2016**, *26*, 258–263. [CrossRef]
83. Wang, Q.; Zhou, C.; Yan, X.H.; Wang, J.J.; Wang, D.F.; Yuan, X.X.; Cheng, X.N. TiO_2 nanoparticles modified MoO_3 nanobelts as electrode materials with superior performances for supercapacitors. *Energy Technol.* **2018**, *6*, 2367–2373. [CrossRef]
84. Chen, J.; Nakate, U.T.; Nguyen, Q.T.; Wei, Y.; Park, S. Surface activated Co_3O_4/MoO_3 nanostructured electrodes by air-plasma treatment toward enhanced supercapacitor. *Mater. Sci. Eng. B* **2022**, *285*, 115928. [CrossRef]
85. Wang, S.-Q.; Cai, X.; Song, Y.; Sun, X.; Liu, X.-X. VO_x@MoO_3 nanorod composite for high-performance supercapacitors. *Adv. Funct. Mater.* **2018**, *28*, 1803901. [CrossRef]
86. Muduli, S.; Pati, S.K.; Swain, S.; Martha, S.K. MoO_3@ZnO nanocomposite as an efficient anode material for supercapacitors: A cost effective synthesis approach. *Energy Fuels* **2021**, *35*, 16850–16859. [CrossRef]
87. Wang, Y.; Zhang, L.; Hou, H.; Xu, W.; Duan, G.; He, S.; Liu, K.; Jiang, S. Recent progress in carbon-based materials for supercapacitor electrodes: A review. *J. Mater. Sci.* **2020**, *56*, 173–200. [CrossRef]
88. Si, H.; Sun, L.; Zhang, Y.; Wu, L.; Zhang, Y.; Zhang, Y. Enhanced pseudocapacitive energy storage properties of budding-branch like MoO_2@C/CNT nanorods. *Dalton Trans.* **2020**, *49*, 1637–1645. [CrossRef]
89. Tiwari, P.; Jaiswal, J.; Chandra, R. Hierarchal growth of MoS_2@CNT heterostructure for all solid state symmetric supercapacitor: Insights into the surface science and storage mechanism. *Electrochim. Acta* **2019**, *324*, 134767. [CrossRef]
90. Tian, Y.; Sarwar, S.; Zheng, Y.; Wang, S.; Guo, Q.; Luo, J.; Zhang, X. Ultrafast microwave manufacturing of MoP/MoO_2/carbon nanotube arrays for high-performance supercapacitors. *J. Solid State Electrochem.* **2020**, *24*, 809–819. [CrossRef]
91. Zhao, Y.; Xing, G.; Liu, H.; Zhang, W.; Liu, Q.; Zhao, C.; Li, Y.; Wang, Y. Facile construction of MoS_2/graphene aerogel composite by depositing MoS_2 film with a magnetron sputtering method for high-performance supercapacitors. *Solid State Commun.* **2022**, *351*, 114789. [CrossRef]
92. Liu, Z.; Qin, A.; Yang, B.; Wang, D.; Zhang, Z. Flower-like MoS_2 onto nitrogen-doped 3D graphene composite with active material for supercapacitor electrodes. *Mater. Lett.* **2019**, *240*, 258–261. [CrossRef]
93. Chen, J.; Jin, T.; Deng, H.; Huang, J.; Ren, G.; Qian, Y. MoO_2 nanoparticles confined in N,P-codoped graphene aerogels with excellent pseudocapacitance performance. *Can. J. Chem.* **2021**, *99*, 303–310. [CrossRef]
94. Qu, G.; Guo, K.; Dong, J.; Huang, H.; Yuan, P.; Wang, Y.; Yuan, H.; Zheng, L.; Zhang, J.-N. Tuning Fe-spin state of FeN_4 structure by axial bonds as efficient catalyst in Li-S batteries. *Energy Storage Mater.* **2023**, *55*, 490–497. [CrossRef]
95. Deng, Y.; Zhao, Y.; Peng, K.; Yu, L. One-step hydrothermal synthesis of MoO_2/MoS_2 nanocomposites as high-performance electrode material for supercapacitors. *ACS Appl. Mater. Interfaces* **2022**, *14*, 49909–49918. [CrossRef] [PubMed]
96. Yang, L.; Huang, M.; Lu, M.; Guan, X.; Guan, X.; Wang, G.; Jia, B. Facile design and synthesis of nickle-molybdenum oxide/sulfide composites with robust microsphere structure for high-performance supercapacitors. *Chem. Eng. J.* **2019**, *364*, 462–474. [CrossRef]
97. Qin, Q.; Chen, L.; Wei, T.; Liu, X. MoS_2/NiS yolk-shell microsphere-based electrodes for overall water splitting and asymmetric supercapacitor. *Small* **2019**, *15*, 1803639. [CrossRef]
98. Liu, Y.; Zheng, Y.; Xu, Q.; Shi, Y.; Tian, Z.; Wang, R.; Zhang, G.; Chen, J.; Wang, Z.; Zheng, W. Controllable synthesis of NiSe/$MoSe_2$/MoO_2 3D hierarchical hollow microspheres with enhanced performance for asymmetric supercapacitors. *Chem. Eng. J.* **2020**, *387*, 124121. [CrossRef]
99. Wang, C.; Wu, D.; Qin, Y.; Kong, Y. Nanowired $NiMoO_4$/$NiSe_2$/$MoSe_2$ prepared through in situ selenylation as a high performance supercapacitor electrode. *Chem. Commun.* **2021**, *57*, 4019–4022. [CrossRef]
100. Krishna, B.N.V.; Ankinapalli, O.R.; Reddy, A.R.; Yu, J.S. Facile one-step hydrothermal route to MSe/Mo_3Se_4 (M: Zn, Mn, and Ni)-based electrode materials for ultralong-life hybrid supercapacitors. *J. Mater. Sci. Technol.* **2023**, *156*, 230–240. [CrossRef]
101. Zhou, G.; Wang, Y.; Huang, Z. Structure and function tailored metal-organic frameworks for heterogeneous catalysis. *Chem. Catal.* **2022**, *2*, 3304–3319. [CrossRef]
102. Zhang, X.; Li, D.; Dong, C.; Shi, J.; Xu, Y. The synergistic supercapacitive performance of Mo-MOF/PANI and its electrochemical impedance spectroscopy investigation. *Mater. Today Commun.* **2019**, *21*, 100711. [CrossRef]
103. Cai, Z.; Deng, L.; Song, Y.; Li, D.; Hong, L.; Shen, Z. Facile synthesis of hierarchically self-assembled dandelion-like microstructures of bimetallic-MOF as a novel electrode material for high-rate supercapacitors. *Mater. Lett.* **2020**, *281*, 128616. [CrossRef]
104. Li, Q.; Guo, H.; Xue, R.; Wang, M.; Xu, M.; Yang, W.; Zhang, J.; Yang, W. Self-assembled Mo doped Ni-MOF nanosheets based electrode material for high performance battery-supercapacitor hybrid device. *Int. J. Hydrogen Energy* **2020**, *45*, 20820–20831. [CrossRef]

105. Gourji, F.H.; Rajaramanan, T.; Kishore, A.; Heggertveit, M.; Velauthapillai, D. Hierarchical cube-in-cube cobalt-molybdenum phosphide hollow nanoboxes derived from the MOF template strategy for high-performance supercapacitors. *ACS Omega* **2023**, *8*, 23446–23456. [CrossRef] [PubMed]
106. Govindan, R.; Hong, X.J.; Sathishkumar, P.; Cai, Y.P.; Gu, F.L. Construction of metal-organic framework-derived CeO_2/C integrated MoS_2 hybrid for high-performance asymmetric supercapacitor. *Electrochim. Acta* **2020**, *353*, 136502. [CrossRef]
107. Safartoobi, A.; Mazloom, J.; Ghodsi, F.E. Silver/molybdenum metal-organic framework derived Ag_2MoO_4 nanoparticles as novel electrode for high-performance supercapacitor. *J. Energy Storage* **2023**, *68*, 107818. [CrossRef]